

Long-range order in two-dimensional systems with fluctuating active stresses

Yann-Edwin Keta* and Silke Henkes†

Instituut-Lorentz for Theoretical Physics, Universiteit Leiden, 2333 CA Leiden, Netherlands

(Dated: 22nd October 2024, 00:11)

In two-dimensional tissues, such as developing germ layers, pair-wise forces (or active stresses) arise from the contractile activity of the cytoskeleton, with dissipation provided by the three-dimensional surroundings. We show analytically how these pair-wise stochastic forces, unlike the particle-wise independent fluctuating forces usually considered in active matter systems, produce conserved centre-of-mass dynamics and so are able to damp large-wavelength displacement fluctuations in elastic systems. A consequence of this is the stabilisation of long-range translational order in two dimensions, in clear violation of the celebrated Mermin-Wagner theorem, and the emergence of hyperuniformity with a structure factor $S(q) \sim q^2$ in the $q \rightarrow 0$ limit. We then introduce two numerical cell tissue models which feature these pair-wise active forces. First a vertex model, in which the cell tissue is represented by a tiling of polygons where the edges represent cell junctions and with activity provided by stochastic junctional contractions. Second an active disk model, derived from active Brownian particles, but with pairs of equal and opposite stochastic forces between particles. We confirm our analytical prediction of long-range order in both numerical models and show that hyperuniformity survives in the disordered phase, thus constituting a hidden order in our model tissue. Owing to the generality of this mechanism, we expect our results to be testable in living organisms, and to also apply to artificial systems with the same symmetry.

I. INTRODUCTION

Biological tissues are a paradigmatic active or living material, characterised by the competition between crowding effects and active driving. In in-vitro epithelial cell layers, the focus of most models, activity arises primarily from cells crawling over the underlying solid substrate [1, 2]. This setup has motivated a number of minimal microscopic models of tissues, such as self-propelled particles [3–6] and self-propelled Voronoi models [7–9]. In these, the “self-propelled” qualifier indicates that a time-persistent and space-independent force acts on each degree of freedom (*e.g.* particle or Voronoi centre). However, in many developmental contexts such as avian [10–12] and drosophila [13] early development, the driving activity arises from cytoskeletal contractility [14–16], and the cells are surrounded by fluid that provides dissipation, but against which the tissue cannot exert active forces. These models therefore are not suitable here, and instead the active interactions within cell sheets need to be modelled as stochastic forces which act on pairs of degrees of freedom in an opposite manner, thus respecting action-reaction. Since the sum of these driving forces cancel, the dynamics they produce conserves the centre of mass, and should be regarded in continuum elastic formulation as deriving from the divergence of an active stress $\underline{\sigma}^{\text{act}}$. We may then write for these overdamped systems

$$\zeta \dot{\mathbf{u}}(\mathbf{r}, t) = - \int d^2 \mathbf{r}' \underline{\mathbf{D}}^{\text{el}}(\mathbf{r} - \mathbf{r}') \mathbf{u}(\mathbf{r}', t) + \nabla \cdot \underline{\sigma}^{\text{act}}(\mathbf{r}, t) \quad (1)$$

where $\mathbf{u}(\mathbf{r}, t)$ describes the elastic deformation from position \mathbf{r} , ζ is a friction coefficient, and $\underline{\mathbf{D}}^{\text{el}}$ is a dynamical matrix [17] describing elasticity (see Fig. 1(a)). More generally, one can envisage a full dissipation matrix $\underline{\zeta}$ that includes additional cell-cell terms, a point we will return to below.

Recent studies within a field theoretical [18] and a granular context [19] have linked stochastic active stresses and the emergence of crystalline phases with long-range translational order and hyperuniform density fluctuations – fluctuations which vanish on large length scales. In the active matter context, long-range translational order and hyperuniformity have also recently been uncovered in systems with anti-alignment [20], chiral or non-reciprocal interactions [21, 22], oscillatory driving forces [23], as well as in active turbulence [24] – see a recent review [25]. However, a full understanding together with a minimal model of these processes is lacking, and the link to the biological context has so far not been made.

It should be noted that within a continuum active fluid paradigm, Eq. (1) with pair forces would belong to the well-understood class of dry or mixed dry-wet active nematics or active gels which have long been proposed as tissue models [26, 27]. The difference here is the active *solid* starting point with purely fluctuating activity, very unlike the typical active nematic state with moving defects. Moreover, we take microscopic order into account, allowing us to access translational and hexatic order parameters – see however [28, 29] for an intrinsically hexatic active fluid approach.

In this paper we first derive the active elastic theory of long-range correlations at linear order. We then show in two models of dense biological tissues how pair-wise fluctuating active forces stabilise long-range translational order. In addition, we show numerically that hyperuni-

* keta@lorentz.leidenuniv.nl

† shenkes@lorentz.leidenuniv.nl

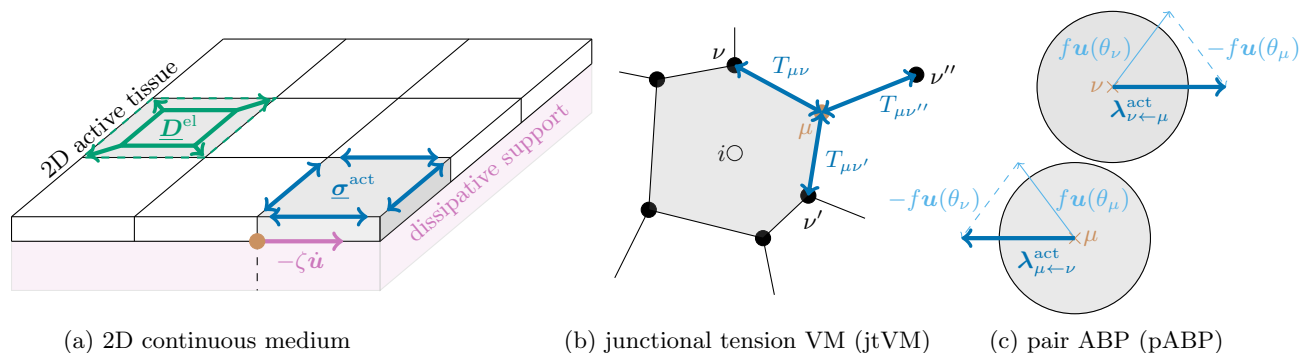


FIG. 1. (a) Sketch of a two-dimensional continuous system with fluctuating active stress described by (1). (b) Vertex model with stochastic junction tension (jtVM). (c) Active Brownian particles with pair-wise propulsion forces (pABP).

formity is displayed both in the low-noise ordered solid and the large-noise disordered liquid, indicating a form of hidden order on large scales. We contrast these results with simulations of analogous models with particle-wise fluctuating active forces where translational order is at most quasi-long-range with algebraically decreasing correlations [30] and diverging structural fluctuations in the infinite size limit. The paper is organised as follows. In Sec. II we derive analytically the structural fluctuations of models described by (1). In Sec. III we introduce our models and perform the numerical study of their structural characteristics. In Sec. IV we gather our findings and discuss their future applications.

II. LONG-RANGE TRANSLATIONAL ORDER AND HYPERUNIFORMITY

At thermal equilibrium, the Mermin-Wagner theorem indicates that there can be no spontaneous breaking of a continuous symmetry in dimensions $d = 1, 2$ at finite temperature [31]. A consequence of this is that thermally induced long-range displacement fluctuations grow with system size in these low dimensions, and long-range translational order is unachievable in the thermodynamic limit [32, 33]. Moving flocks however (almost certainly [34]) display true long-range polar *orientational* order [35], the first indication that activity allows for exceptions of this law.

Structural fluctuations can be quantified through the counting of the number $N(R)$ of particles in a volume R^d as a function of R . For typical disordered systems such as liquids, the variance $\text{Var}(N; R) = \langle N(R)^2 \rangle - \langle N(R) \rangle^2$ grows as R^d , while $\text{Var}(N; R) \sim R^{d-1}$ in periodic crystals [36]. Many active systems, in particular those which display flocking behaviours, were reported to display *giant number fluctuations*, in the sense that $\text{Var}(N; R)$ grows faster than R^d [37–42]. More recently, long-range translational order in two-dimensional active systems has been a subject of interest. Galliano *et al.* have shown how such order arises in a nonequilibrium particle model driven by pair-wise random displacements [43], and Maire and

Plati have studied this property in systems driven by a momentum-conserving noise [19]. In both cases, long-range translational order is associated with *hyperuniformity*. This designates the anomalous vanishing of density fluctuations on large length scales [44], associated with a variance $\text{Var}(N; R)$ which decreases slower than R^d , and is known to occur in systems with absorbing state transitions [45–47].

In this Section we derive, for a two-dimensional continuous elastic medium, the fluctuations of the displacement field at linear order. In a second part we show how these relate, in a discrete system, to the translational order correlation function and the scaling of the structure factor over large wavelengths.

A. Two-dimensional continuous medium

We introduce the Fourier transform in space and time of the displacement field

$$\begin{aligned} \mathbf{u}(\mathbf{r}, t) &= \int d^2\mathbf{q} e^{-i\mathbf{q}\cdot\mathbf{r}} \tilde{\mathbf{u}}(\mathbf{q}, t) \\ &= \int d^2\mathbf{q} \int d\omega e^{-i\mathbf{q}\cdot\mathbf{r} - i\omega t} \tilde{\mathbf{U}}(\mathbf{q}, \omega), \end{aligned} \quad (2)$$

and write (1) in Fourier space as

$$-i\omega\zeta\tilde{\mathbf{U}}(\mathbf{q}, \omega) = -\tilde{\mathbf{D}}^{\text{el}}(\mathbf{q})\tilde{\mathbf{U}}(\mathbf{q}, \omega) + \tilde{\mathbf{\Lambda}}(\mathbf{q}, \omega), \quad (3)$$

where $\tilde{\mathbf{\Lambda}}(\mathbf{q}, \omega)$ is the Fourier transform of the noise term

$$\boldsymbol{\lambda}(\mathbf{r}, t) = \nabla \cdot \boldsymbol{\sigma}^{\text{act}}(\mathbf{r}, t). \quad (4)$$

We assume (i) that the Fourier transform of the dynamical matrix $\tilde{\mathbf{D}}^{\text{el}}(\mathbf{q})$ can be decomposed as follows [5]

$$\begin{aligned} \tilde{\mathbf{D}}^{\text{el}}(\mathbf{q})\tilde{\mathbf{U}}(\mathbf{q}, \omega) &= |\mathbf{q}|^2 \left[(B + \mu)\tilde{\mathbf{U}}_{\parallel}(\mathbf{q}, \omega) + \mu\tilde{\mathbf{U}}_{\perp}(\mathbf{q}, \omega) \right], \end{aligned} \quad (5)$$

where $\hat{\mathbf{q}} = \mathbf{q}/|\mathbf{q}|$, $\tilde{\mathbf{U}}_{\parallel}(\mathbf{q}, \omega) = (\tilde{\mathbf{U}}(\mathbf{q}, \omega) \cdot \hat{\mathbf{q}})\hat{\mathbf{q}}$ and $\tilde{\mathbf{U}}_{\perp}(\mathbf{q}, \omega) = \tilde{\mathbf{U}}(\mathbf{q}, \omega) - \tilde{\mathbf{U}}_{\parallel}(\mathbf{q}, \omega)$ are respectively the

longitudinal and transverse displacements in Fourier space, and B and μ are respectively the bulk and shear moduli.

We assume (ii) that the fluctuations of the active stress (4) follow [18, 19, 48]

$$\langle \boldsymbol{\lambda}(\mathbf{r}, t) \cdot \boldsymbol{\lambda}(\mathbf{r}', t') \rangle = -\sigma^2 a^2 e^{-|t-t'|/\tau} \nabla^2 \delta(\mathbf{r} - \mathbf{r}'), \quad (6)$$

where σ is an energy scale, a a coarse-graining length scale, and τ a persistence time. This assumption stems from the idea that the stress is uncorrelated in space but autocorrelated in time. We highlight here that, from the point of view of numerical particle-based models, the

divergence of the stress in (4) should be interpreted as the discrete divergence of a noise vector field defined over the ensemble of pairs of particles [48]. Assuming that these noise vectors are uncorrelated between pairs leads to (6) with ∇^2 interpreted as a discrete Laplacian. We provide an exact derivation for a triangular lattice in Appendix B. We write (6) in Fourier space as

$$\langle \tilde{\boldsymbol{\Lambda}}(\mathbf{q}, \omega) \cdot \tilde{\boldsymbol{\Lambda}}(\mathbf{q}', \omega')^* \rangle = \frac{2\sigma^2 a^2 |\mathbf{q}|^2}{1 + \omega^2 \tau^2} \delta(\mathbf{q} - \mathbf{q}'). \quad (7)$$

We use (3), (5), and (7), to compute the equal-time displacement fluctuations in Fourier space (see Appendix A for a full derivation) and obtain

$$\langle \tilde{\mathbf{u}}(\mathbf{q}, t) \cdot \tilde{\mathbf{u}}(\mathbf{q}', t)^* \rangle = \frac{2\pi\sigma^2\tau^2}{\zeta^2} \left[\frac{\xi_{\parallel}^{-2}}{1 + |\mathbf{q}|^2 \xi_{\parallel}^2} + \frac{\xi_{\perp}^{-2}}{1 + |\mathbf{q}|^2 \xi_{\perp}^2} \right] a^2 \delta(\mathbf{q} - \mathbf{q}'), \quad (8a)$$

where we have used the longitudinal and transversal correlation length scales $\xi_{\parallel} = \sqrt{(B + \mu)\tau/\zeta}$ and $\xi_{\perp} = \sqrt{\mu\tau/\zeta}$. We compare this result to the case of a space-uncorrelated fluctuating force field with correlations $\langle \boldsymbol{\lambda}(\mathbf{r}, t) \cdot \boldsymbol{\lambda}(\mathbf{r}', t') \rangle = f^2 a^2 e^{-|t-t'|/\tau} \delta(\mathbf{r} - \mathbf{r}')$, for which the spectrum reads [5]

$$\langle \tilde{\mathbf{u}}(\mathbf{q}, t) \cdot \tilde{\mathbf{u}}(\mathbf{q}', t)^* \rangle = \frac{2\pi f^2 \tau^2}{\zeta^2} \frac{1}{|\mathbf{q}|^2} \left[\frac{\xi_{\parallel}^{-2}}{1 + |\mathbf{q}|^2 \xi_{\parallel}^2} + \frac{\xi_{\perp}^{-2}}{1 + |\mathbf{q}|^2 \xi_{\perp}^2} \right] a^2 \delta(\mathbf{q} - \mathbf{q}'). \quad (8b)$$

Spectrum (8a) importantly differs from (8b) by the absence of the factor $1/|\mathbf{q}|^2$ which diverges on large length scales $|\mathbf{q}| \rightarrow 0$. This difference arises solely from the spectrum of stochastic forces (7) whose fluctuations vanish in the limit $|\mathbf{q}| \rightarrow 0$.

We define the variance of displacement for a square two-dimensional system of linear size L as

$$\langle u^2 \rangle = \lim_{t \rightarrow \infty} \iint_{2\pi/L}^{\infty} d^2\mathbf{q} d^2\mathbf{q}' \langle \tilde{\mathbf{u}}(\mathbf{q}, t) \cdot \tilde{\mathbf{u}}(\mathbf{q}', t)^* \rangle. \quad (9)$$

The difference in \mathbf{q} -scaling we have stressed between spectra (8) leads to the following respective variances scaling in the thermodynamic limit

$$\langle u^2 \rangle_{L \rightarrow \infty}^{\sigma} = \langle u^2 \rangle_{\infty}^{\sigma} = \text{cst}, \quad (10a)$$

$$\langle u^2 \rangle_{L \rightarrow \infty}^f = C^f \log(L/a). \quad (10b)$$

where the σ and f subscript refer to the fluctuating stress and force cases respectively. In the latter case of a fluctuating force field, this variance diverges for infinite systems [19, 49].

B. Two-dimensional regular lattice

We just showed how two-dimensional systems with fluctuating active stresses have finite displacement fluctua-

tions in the thermodynamic limit $L \rightarrow \infty$. This motivates us to investigate structural fluctuations in discrete ordered systems. We then consider a system of N particles with displacements $\mathbf{u}_i = \mathbf{r}_i - \mathbf{r}_i^0$ from their equilibrium lattice points \mathbf{r}_i^0 . We highlight that the displacement spectra (8) follow the transformation from continuous to discrete Fourier space $\langle \tilde{\mathbf{u}}(\mathbf{q}, t) \cdot \tilde{\mathbf{u}}(\mathbf{q}', t)^* \rangle \rightarrow \langle \tilde{\mathbf{u}}_{\mathbf{q}}(t) \cdot \tilde{\mathbf{u}}_{\mathbf{q}'}(t)^* \rangle$ through a change of factor $a^2 \delta(\mathbf{q} - \mathbf{q}') \rightarrow N \delta_{\mathbf{q}, \mathbf{q}'}$ [5], with the coarse-graining length scale defined as $a = L/\sqrt{N}$.

We introduce the local hexatic orientational order parameter $\psi_{6,i}$ and the local translational order parameter $\psi_{\mathbf{q}_0,i}$ in order to quantify structural order [30, 50–52],

$$\psi_{6,i} = \frac{1}{z_i} \sum_{j \in \mathcal{N}_i} e^{6i\theta_{ij}}, \quad \theta_{ij} = \arg(\mathbf{r}_j - \mathbf{r}_i), \quad (11)$$

$$\psi_{\mathbf{q}_0,i} = e^{i\mathbf{q}_0 \cdot (\mathbf{r}_i - \mathbf{r}_0)}, \quad (12)$$

where \mathcal{N}_i is the ensemble of nearest neighbours of particle i and z_i the coordination number of particle i *i.e.* the number of particles in \mathcal{N}_i , \mathbf{r}_0 is the position of one of the particles, and \mathbf{q}_0 is a reciprocal vector of the lattice. We infer the latter from the position of the maximum of the structure factor (16) $S(\mathbf{q}_0) = \max_{\mathbf{q}} S(\mathbf{q})$ [53].

The translation by $-\mathbf{r}_0$ in (12) is chosen so that $\psi_{\mathbf{q}_0,i} = 1$ everywhere in a perfect crystal lattice (see Fig. 3). This works since for any vector \mathbf{v} between two

lattice points that $\mathbf{q}_0 \cdot \mathbf{v}$ is 0 modulo 2π . As this simply corresponds to choosing a particular origin, it does not affect the correlations (14), only the argument of (12).

We quantify the global order parameter with the following ensemble averages ($x = 6, \mathbf{q}_0$)

$$\Psi_x = \left\langle \left| \frac{1}{N} \sum_{i=1}^N \psi_{x,i} \right| \right\rangle, \quad (13)$$

and the following spatial correlation functions

$$C_x(r) = \left\langle \frac{\sum_{i \neq j} \psi_{x,i} \psi_{x,j}^* \delta(r - |\mathbf{r}_j - \mathbf{r}_i|)}{\sum_{i \neq j} \delta(r - |\mathbf{r}_j - \mathbf{r}_i|)} \right\rangle. \quad (14)$$

The latter function, considering translational order, is related to the scalings (10) (see Appendix C) as follows

$$C_{\mathbf{q}_0}^\sigma(r) \underset{L \rightarrow \infty}{\underset{r \rightarrow \infty}{=}} e^{-\frac{1}{2} |\mathbf{q}_0|^2 \langle u^2 \rangle_\infty^\sigma}, \quad (15a)$$

$$C_{\mathbf{q}_0}^f(r) \underset{L \rightarrow \infty}{\underset{r \rightarrow \infty}{\sim}} r^{-\frac{1}{2} |\mathbf{q}_0|^2 C^f}. \quad (15b)$$

These scalings show that, in the case a stochastic stress field, *true* long-range translational order is possible, as opposed to the quasi-long-range order in the case of a stochastic force field.

Finally, we define the structure factor [54]

$$S(\mathbf{q}) = \frac{1}{N} \sum_{i,j=1}^N \left\langle e^{i\mathbf{q} \cdot (\mathbf{r}_j - \mathbf{r}_i)} \right\rangle \quad (16)$$

which characterises density fluctuations. Under the assumptions of normally distributed displacements (*e.g.* satisfied for normally distributed stochastic forces and harmonic interactions) and isotropy, the structure factor can be reduced in the large system size and large wavelength limit to (see Appendix D for a derivation)

$$S(\mathbf{q}) \underset{L \rightarrow \infty}{\underset{|\mathbf{q}| \sim 2\pi/L}{=}} \frac{1}{2N} |\mathbf{q}|^2 \langle |\tilde{\mathbf{u}}_{\mathbf{q}}|^2 \rangle. \quad (17)$$

Therefore, given the displacement spectra (8), we infer the following scalings for the structure factor (16)

$$S^\sigma(\mathbf{q}) \underset{L \rightarrow \infty}{\underset{|\mathbf{q}| \sim 2\pi/L}{\sim}} |\mathbf{q}|^2, \quad (18a)$$

$$S^f(\mathbf{q}) \underset{L \rightarrow \infty}{\underset{|\mathbf{q}| \sim 2\pi/L}{\sim}} 1, \quad (18b)$$

indicating that, in the case of a stochastic stress field, the system is “maximally hyperuniform” similarly to other systems with conserved centre-of-mass dynamics [18, 44–46].

In summary, we have presented three emerging properties for two-dimensional systems in the thermodynamic limit: finite displacement fluctuations with respect to

the lattice positions (10a), long-range translational order (15a), and hyperuniformity (18a). These properties derive from considering a space-uncorrelated stochastic stress field rather than a force field: they rely on the driving fluctuations (here the active stress field) decaying on large wavelengths while competing against a dissipation mechanism acting independently on all individuals in the system. It is noteworthy that these properties would disappear if we included a white noise term in (1) (see Appendix B) – such a term would be expected to counterbalance the white drag if the system were to follow the second fluctuation-dissipation theorem [55–57]. These properties are however not affected if we include an additional viscosity-like cell-cell dissipation term, *i.e.* a full dissipation matrix $\underline{\zeta}$. This adds realism to cell models as it counterbalances the fluctuating stresses, and we can show that this modification as expected only affects the small-wavelength fluctuations (see Appendix B).

III. TISSUE MODELS WITH PAIR-WISE STOCHASTIC FORCES

Our predictions were derived for harmonic systems with particles arranged in regular lattices, and so are potentially susceptible to renormalisation group flow to different exponents from nonlinear terms [18, 47]. In order to test the robustness of these predictions outside of the linear and ordered regime, as well as the applicability of these results, we introduce two numerical models suited for the description of dense cell tissues (see Fig. 1) and study their structural fluctuations.

A. Model definitions

In Sec. III A 1, we introduce a model based on a polygonal tiling of the two-dimensional space, where each tile represents a single cell. This kind of model has been widely used to represent confluent cell sheets [2, 58, 59] and allows to represent complex interactions, between cells and between cells and their substrate, as well as constraints on cell shapes. We highlight here two general classes of these models: Voronoi models [7–9, 60] where the tiling of cells is determined through a Voronoi tessellation from cell centres, and vertex models (VM) [61–63] where cell corners (or *vertices*) are the degrees of freedom. The model we first introduce belongs to this second class.

In Sec. III A 2, we introduce a model based on interacting disks. Despite such models lacking the possibility to represent accurate cell shapes and deformations, they have been applied with great success to understand mesoscale correlations in active tissues [5]. Moreover, the simplicity of these models allow for the numerical simulation of the large systems needed to characterise long wavelength fluctuations.

For both models studied here, we introduce the following overdamped equation of motion of their degrees

of freedom (respectively cell vertices and disk centres), which is the discrete analogue of (1),

$$\zeta \dot{\mathbf{r}}_\mu = -\partial_{\mathbf{r}_\mu} U^{\text{int}} + \boldsymbol{\lambda}_\mu^{\text{act}}, \quad (19)$$

where the degrees of freedom are indexed by μ , ζ is a friction coefficient, U^{int} is an interaction potential, and the $\boldsymbol{\lambda}_\mu^{\text{act}}$ are the active driving forces.

1. Junctional tension vertex model (jtVM)

Vertex models are defined as meshes of vertices μ , at positions \mathbf{r}_μ , linked by edges which enclose faces which describe the cells i (see Fig. 1(b)). By extension we will denote i the centroid of cell i , whose position is

$$\mathbf{r}_i = \frac{1}{6A_i} \sum_{\mu \in \text{cell } i} (\mathbf{r}_\mu + \mathbf{r}_{\mu+1})(x_\mu y_{\mu+1} - x_{\mu+1} y_\mu), \quad (20)$$

where $\mathbf{r}_\mu = (x_\mu, y_\mu)$, vertices μ are ordered in an anti-clockwise direction relative to the cell centre i , and where A_i is the area of cell i ; we denote its perimeter by P_i . We stress that the centroid corresponds to the centre of mass of the cell, *i.e.* the arithmetic mean of all the points on its surface, and should be distinguished from the mean of its corners' positions.

We introduce the following vertex model interaction potential [60]

$$U^{\text{int}} = \sum_{\text{cells } i} \left[\frac{1}{2} \frac{k}{A_0} (A_i - A_0)^2 + \frac{1}{2} k (P_i - P_0)^2 \right], \quad (21)$$

with k a spring constant, A_0 the target area and P_0 the target perimeter.

We consider active forces which are pair-wise or particle-wise, respectively (see Fig. 1(b) for a visual representation)

$$\boldsymbol{\lambda}_\mu^{\text{act}} = \sum_{\nu \wedge \mu} T_{\mu\nu} \hat{\boldsymbol{\ell}}_{\mu\nu}, \quad (22a)$$

$$\boldsymbol{\lambda}_\mu^{\text{act}} = f \mathbf{u}(\theta_\mu), \quad (22b)$$

where f is the stochastic force amplitude, $\mathbf{u}(\theta_\mu) = (\cos \theta_\mu, \sin \theta_\mu)$, $\nu \wedge \mu$ designates the vertices ν linked by an edge to vertex μ , $T_{\mu\nu}$ is the tension of edge $\mu\nu$, $\boldsymbol{\ell}_{\mu\nu} = \mathbf{r}_\nu - \mathbf{r}_\mu$ and $\hat{\boldsymbol{\ell}}_{\mu\nu} = \boldsymbol{\ell}_{\mu\nu}/|\boldsymbol{\ell}_{\mu\nu}|$. These forces evolve stochastically: tensions $T_{\mu\nu}$ follow an Ornstein-Uhlenbeck process [64–67] and angles θ_μ diffuse similarly to self-propelled Voronoi models [8, 9],

$$\tau \dot{T}_{\mu\nu} = -T_{\mu\nu} + \sqrt{2f^2\tau} \eta_{\mu\nu}, \quad (23a)$$

$$\dot{\theta}_\mu = \sqrt{1/\tau} \eta_\mu, \quad (23b)$$

where τ is the persistence time, and $\eta_{\mu\nu}$ and η_μ are Gaussian white noises with zero means and variances $\langle \eta_{\mu\nu}(0) \eta_{\alpha\beta}(t) \rangle = \delta_{\mu\alpha} \delta_{\nu\beta} \delta(t)$ and $\langle \eta_\mu(0) \eta_\nu(t) \rangle = \delta_{\mu\nu} \delta(t)$.

We perform simulations of N cells with periodic boundary conditions. We define the unit length $\sqrt{A_0} = 1$, energy $kA_0 = 1$, and time $\zeta/k = 1$. Simulations are started from a regular hexagonal packing which satisfies cell areas $A_i = A_0$. This implies that the area of the system is $L^2 = NA_0$. We enforce the shape index $s_0 = P_0/\sqrt{A_0} = 3.72$ such that in absence of forcing the regular hexagonal packing of cells is both rigid and force-free. We use $\tau = 5$ for all data presented.

This model is integrated using the MIT-licensed library `cells` [68].

2. Pair active Brownian particles (pABP)

We consider N disk particles with diameters D and positions \mathbf{r}_μ which interact via a harmonic pair-wise potential

$$U^{\text{int}} = \sum_{\substack{\mu, \nu=1 \\ \mu \neq \nu}}^N \frac{1}{2} k (D - |\mathbf{r}_\nu - \mathbf{r}_\mu|)^2 \Theta(D - |\mathbf{r}_\nu - \mathbf{r}_\mu|), \quad (24)$$

where Θ is the Heaviside function. For this model the cell centres are the disk centres with positions $\mathbf{r}_i = \mathbf{r}_\mu$.

We consider active forces which are pair-wise or particle-wise, respectively (see Fig. 1(c) for a visual representation)

$$\boldsymbol{\lambda}_\mu^{\text{act}} = f \sum_{\substack{\nu=1 \\ \mu \neq \nu}}^N (\mathbf{u}(\theta_\mu) - \mathbf{u}(\theta_\nu)) \beta(|\mathbf{r}_\nu - \mathbf{r}_\mu|), \quad (25a)$$

$$\boldsymbol{\lambda}_\mu^{\text{act}} = f \mathbf{u}(\theta_\mu), \quad (25b)$$

where f is the stochastic force amplitude and with the kernel function $\beta(r) = (1 - r/D')\Theta(D' - r)$ where $D' = 1.5D > D$ to avoid singularities at the point of contact. These forces evolve stochastically: angles θ_μ diffuse as in active Brownian particles [3, 4, 69]

$$\dot{\theta}_\mu = \sqrt{1/\tau} \eta_\mu, \quad (26)$$

where τ is the persistence time, and η_μ is a Gaussian white noise with zero mean and variance $\langle \eta_\mu(0) \eta_\nu(t) \rangle = \delta_{\mu\nu} \delta(t)$. We stress that the particle-wise force model corresponds exactly to active Brownian particles (ABPs).

We perform simulations of N cells with periodic boundary conditions. We define the unit length $D/2 = 1$, energy $k(D/2)^2 = 1$, and time $\zeta/k = 1$. Simulations are started from a regular hexagonal packing with packing fraction $\phi = N\pi(D/2)^2/L^2 = 1$, corresponding to a thoroughly solid state. We use $\tau = 25$ for all data presented.

This model is integrated using the GPL-licensed library `SAMoS` [70].

B. Location of the transition

We expect a disordered *liquid* phase at large stochastic force amplitude f , and an ordered *solid* phase at small

f . While in equilibrium, it is expected that structural and dynamical characteristics coincide and so determine the phase of the system, we cannot exclude that out of equilibrium, structure and dynamics may indicate different phases (see e.g. the flowing crystals of [71]). We thus consider two structural characteristics, the global hexatic and translational order parameters Ψ_6 and Ψ_{q_0} (13), and a dynamical characteristics, the mean square displacement (MSD) [72]

$$\text{MSD}(t) = \frac{1}{N} \sum_{i=1}^N \langle |[\mathbf{r}_i(t) - \bar{\mathbf{r}}(t)] - [\mathbf{r}_i(0) - \bar{\mathbf{r}}(0)]|^2 \rangle, \quad (27)$$

with $\bar{\mathbf{r}}(t) = (1/N) \sum_{i=1}^N \mathbf{r}_i(t)$ the position of the centre of mass at time t , to determine the phase of our models as a function of the force amplitudes.

For both jtVM and pABP models there is, as the force amplitude is decreased, a sharp simultaneous increase in both translational and hexatic order (Fig. 2(a, b)). We thus observe a structurally ordered phase, in the jtVM model for $f \lesssim 0.03$, and in the pABP model for $f \lesssim 0.11$. This structural ordering coincides with a dynamical transition from a diffusing liquid state at large f , where correlations decay over times $t \gtrsim \tau$, to an arrested solid

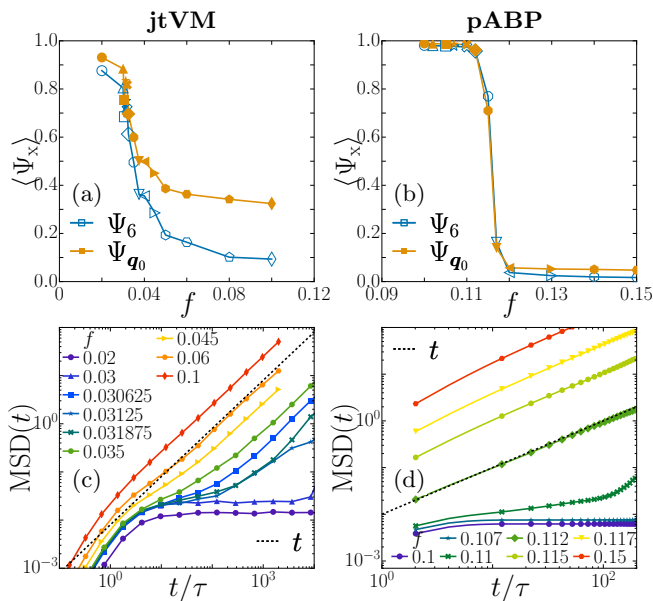


FIG. 2. (a, b) Global structural order parameters (13) – hexatic order parameter Ψ_6 (blue open symbols) and translational order parameter Ψ_{q_0} (orange full symbols) – in steady state as functions of the stochastic force amplitude f . (c, d) Mean squared displacements as functions of time $\text{MSD}(t)$ (27) in steady state for different stochastic force amplitudes f . Dashed lines are linear functions of time as guides to the eye. (a, c) Junctional tension vertex model (jtVM) with $N = 108$ cells and persistence time $\tau = 5$. (b, d) Pair active Brownian particles (pABP) with $N = 16384$ particles and persistence time $\tau = 25$. Identical markers between (a) and (c) and between (b) and (d) correspond to identical data sets.

state at small f as evidenced by the plateau in MSD (Fig. 2(c, d)). As a matter of comparison, we also provide the dynamical characteristics of the ABP model in Appendix E.

In Fig. 3, we plot configurations of the pABP model corresponding to the solid (a, b), the liquid (e, f), and a configuration at an intermediate value of f (c, d). We confirm that the diffusing liquid state corresponds to a molten state with short-range structural correlations,

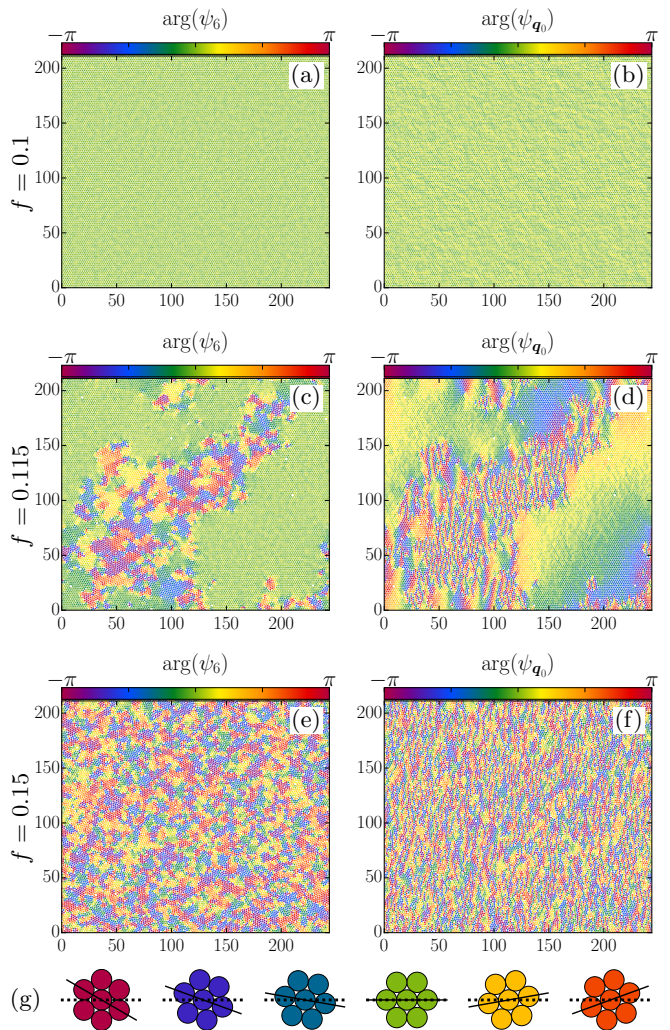


FIG. 3. Order and disorder for pair active Brownian particles (pABP). Visualisation of the argument of the local hexatic order parameter $\arg(\psi_{6,i})$ (11) (left column, (a, c, e)), and the argument of the local translational order parameter $\arg(\psi_{q_0,i})$ (12) (right column, (b, d, f)). (g) shows different hexagonal packing orientations with the colour corresponding to the argument of the hexatic order parameter. Colours associated to the argument of the translational order parameter illustrate deviations from the regular lattice corresponding to ψ_{q_0} : an ordered lattice should display $\arg(\psi_{q_0,i}) = 0$ everywhere. We used $N = 16384$ particles and persistence time $\tau = 25$. Stochastic force amplitude is (a, b) $f = 0.1$, (c, d) $f = 0.115$, (e, f) $f = 0.15$.

while the arrested solid state displays long-range structural order, which we discuss further in Sec. III C. The intermediate force amplitude $f = 0.115$ shows phase coexistence. This appears to be metastable, with the molten state slowly nucleating from the crystalline state (see Appendix F), and we expect the system to show hysteresis. We note that together with the equally abrupt transition in the MSD this is indicative of a first-order phase transition, whose details are however beyond the scope of this paper.

Finally we stress that regions with short-range structural order are rich in defects, as evidenced by coordination numbers $z_i \neq 6$, while regions with long-range structural order are exempt of these same defects (see Appendix G), in accordance with the established understanding of the melting of two-dimensional solids [73]. However, at our current level of description, it is not possible to validate or refute the existence of an *hexatic* phase [8, 74, 75], with finite hexatic order and vanishing translational order (see Appendix H).

C. Structural fluctuations

Deep in the solid phase, we expect our derivations for harmonic lattices to hold.

We first compute the displacement variance $\langle u^2 \rangle$ for both models in the solid phase, with particle-wise and pair-wise stochastic forces, as a function of system size (Fig. 4(a, b)). These confirm our predictions (10). For systems with pair-wise stochastic forces, $\langle u^2 \rangle$ converges to a finite value at large N . In contrast, for systems with particle-wise stochastic forces, $\langle u^2 \rangle$ diverges as $\log L \sim \log \sqrt{N}$. We fit $\langle u^2 \rangle(N)$ to a constant $\langle u^2 \rangle_\infty^\sigma$ for models with pair-wise stochastic forces, and to $C^f \log \sqrt{N}$ for models with particles-wise stochastic forces. We extract $C^f \approx 4.83 \times 10^{-3}$ and $\langle u^2 \rangle_\infty^\sigma \approx 7.00 \times 10^{-3}$ in the vertex model with self-propelled vertices and junction tensions respectively (Fig. 4(a)), and $C^f \approx 2.41 \times 10^{-2}$ and $\langle u^2 \rangle_\infty^\sigma \approx 3.10 \times 10^{-3}$ for active and pair active Brownian particles respectively (Fig. 4(b)).

Next, we compute the translational order correlation function C_{q_0} in the solid phase (Fig. 4(c, d)). We confirm that the solid phase of the models with pair-wise stochastic forces exhibits long-range translational order, with a large-distance correlation value deriving from the (finite) displacement variance. We observe, in the case of particle-wise stochastic forces, that correlations decay algebraically, consistently with quasi-long-range translational order [30]. Our linear response predictions (15) fit this data if we use the values of C^f and $\langle u^2 \rangle_\infty^\sigma$ determined from the system-size dependence of displacement fluctuations (Fig. 4(a, b)), where we also use the measured reciprocal lattice vector squared norms $|\mathbf{q}_0|^2 \approx 45.6$ for the vertex model and $|\mathbf{q}_0|^2 \approx 14.6$ for the particle model. Therefore, we confirm that the exponent of this decay is directly related to the factor with which the displacement

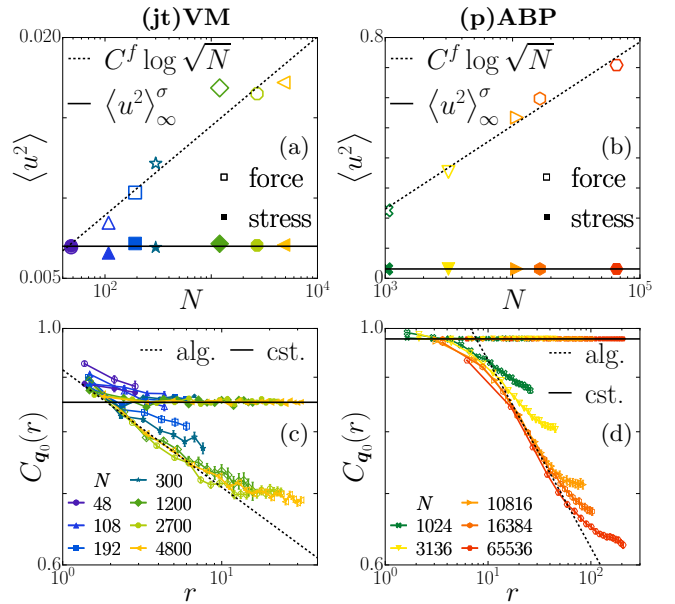


FIG. 4. (a, b) Displacement fluctuations $\langle u^2 \rangle$ (10) computed in steady state and plotted for (a) the vertex model with particle based and junctional tension (jtVM), and (b) particle and pair active Brownian particles (pABP) as a function of the number of particles N . Full symbols represent models with pair-wise stochastic forces, which we fit to a constant $\langle u^2 \rangle_\infty^\sigma$ (solid lines). In contrast, for models with particle-wise stochastic forces (plotted in open symbols), we fit to $C^f \log \sqrt{N}$ (dashed lines). These plots are logarithmic on the x-axis and linear on the y-axis. (c, d) Translational order correlations C_{q_0} (14) for the same data as in (a, b) with pair-wise models (full symbols) and particle-wise models (open symbols), together with our predictions for the large-distance scalings of the correlations (15): a constant (cst., solid lines) for pair-wise and an algebraic decay (alg., dashed lines) for particle-wise stochastic forces. These plots are logarithmic on both axes. We used persistence time $\tau = 5$ and force amplitude $f = 0.02$ for both vertex models (a, c) and persistence time $\tau = 25$ and force amplitudes $f = 0.1$ and $f = 0.05$ for the pair-wise and particle-wise particle models respectively (b, d). Identical colours and markers between plots correspond to identical data sets.

variance diverges (15b).

Finally, we compute the radially-averaged structure factor $S(q)$ to test our predictions of hyperuniformity (16). We present results exclusively for the (p)ABP models because the large systems sizes needed to observe the large-wavelength decay of structural fluctuations are not yet attainable with our current vertex model algorithm. In Fig. 5, we plot the structure factor for particle-wise (a) and pair-wise (b) stochastic forces. In the former case, we observe that $S(q)$ converges to a finite constant as $q \rightarrow 0$, which is the expected behaviour for self-propelled particles systems at moderate activities away from spontaneous phase separation [76, 77]. In the latter case, we do observe the expected scaling $S(q) \sim q^2$ as $q \rightarrow 0$, which confirms that these systems are indeed hyperuni-

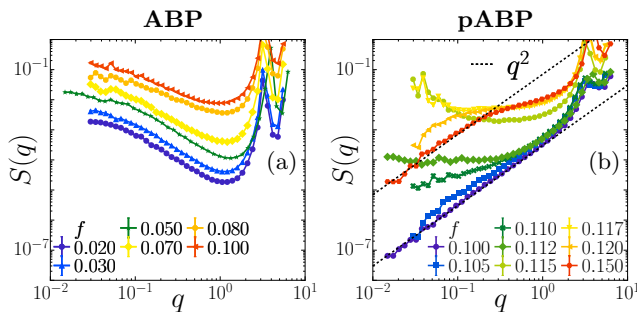


FIG. 5. Structure factor $S(q)$ (16) defined as cylindrical average of $S(\mathbf{q})$ over wave-vectors $\mathbf{q} = (2\pi m/L_x, 2\pi n/L_y)$ which satisfy $|\mathbf{q}| \in [q - \delta q/2, q + \delta q/2]$ with $\delta q = 10^{-2}$. We plot the structure factor for different stochastic force amplitudes f in (a) for the particle model with particle-wise stochastic force (ABP), and in (b) for the particle model with pair-wise stochastic forces (pABP). We used $N = 16384$ or 65536 particles, and persistence $\tau = 25$.

form. Most interestingly, we observe that this scaling applies not only in the solid phase at $f = 0.1$, where our derivation is expected to hold, but also in the liquid phase at $f = 0.15$. Therefore, despite this phase showing orientational and translational disorder on small length scales only (Fig. 3(e, f)), this measurement confirms that there is a “hidden order” on large length scales [36], which has also recently been observed in phase separating droplets [78]. Meanwhile, within the transition region where order and disorder coexist, the system displays more complex, but not hyperuniform scaling of $S(q)$.

IV. DISCUSSION AND CONCLUSION

In this paper we first demonstrated how, within linear elasticity theory, two-dimensional active solids featuring fluctuating active stresses display finite displacement fluctuations $\langle u^2 \rangle$ in the thermodynamic limit $N \rightarrow \infty$ (10), long-range translational order (15), and vanishing large-wavelength density fluctuations, *i.e.* hyperuniformity (18).

These properties derive from, on the one hand, the absence of particle-wise white noise counterbalancing the instantaneous particle-wise friction, thus violating the second fluctuation-dissipation theorem [55–57], and on the other hand, the fluctuations of the driving force vanishing for large wavelengths (7).

Microscopically, these fluctuating active stresses take

the form of pair-wise stochastic forces, forces which respect action-reaction rather than the more usual particle-wise active driving. We introduced two numerical models which incorporate these pair-wise stochastic forces: a vertex model with fluctuating junction tension (jtVM) and a particle-based model with pair-wise additive stochastic forces respecting action-reaction (pABP). We showed that all of our predictions held in both models. These models are built from widespread active matter models used to describe the physics of dense cell tissues, therefore we expect these results to shed light on both out-of-equilibrium ordering transitions as well as on structural fluctuations of living systems.

Since an ordered symmetry-broken phase is possible within our model, it is questionable if the two-step melting scenario of two-dimensional solid from the KTHNY theory applies here. To the best of our current numerical efforts, we have not been able to identify a hexatic phase which would feature short-range translational order and quasi-long-range orientational order. Moreover we observe phase-separated configurations close to the transition (Fig. 3(c, d)) which may indicate a first-order transition between a disordered liquid and an ordered solid as in three-dimensional equilibrium systems.

Our numerical results also show that disordered liquid states, outside the scope of linear elasticity theory, display hyperuniformity as well. While studies have investigated suppressed density fluctuations in force-balanced configurations (ground states of the potential energy) of biological tissue models [79–81], our study provides a new pathway to hyperuniform states in non-arrested phases of such models. Moreover, we note that there is evidence of hyperuniform organisation in biological systems, *e.g.* cell nuclei in brain tumours [82] or suspensions of algae [83]. Further studies may explore if the mechanism we have described is exploited in cell tissues in order to suppress density fluctuations.

V. ACKNOWLEDGEMENTS

We wholeheartedly thank Konstantinos Andreadis, Calvin Bakker, Arthur Hernandez, Sander Kammeraat, Juliane Klamsner, Marko Popović, Jan Rozman, and Rastko Sknepnek for insightful discussions. We acknowledge fruitful discussions at the workshop “Computational Advances in Active Matter” held at the Lorentz Center in Leiden which we thank.

[1] Xavier Trepát, Michael R. Wasserman, Thomas E. Angelini, Emil Millet, David A. Weitz, James P. Butler, and Jeffrey J. Fredberg, “Physical forces during collective cell migration,” *Nature Physics* **5**, 426–430 (2009).

[2] Ricard Alert and Xavier Trepát, “Physical Models of Collective Cell Migration,” *Annual Review of Condensed Matter Physics* **11**, 77–101 (2020).

[3] A. P. Solon, M. E. Cates, and J. Tailleur, “Active brownian particles and run-and-tumble particles: A compar-

- tive study,” *The European Physical Journal Special Topics* **224**, 1231–1262 (2015).
- [4] P. Romanczuk, M. Bär, W. Ebeling, B. Lindner, and L. Schimansky-Geier, “Active Brownian particles: From individual to collective stochastic dynamics,” *The European Physical Journal Special Topics* **202**, 1–162 (2012).
 - [5] Silke Henkes, Kaja Kostanjevec, J. Martin Collinson, Rastko Sknepnek, and Eric Bertin, “Dense active matter model of motion patterns in confluent cell monolayers,” *Nature Communications* **11**, 1405 (2020).
 - [6] David Martin, Jérémy O’Byrne, Michael E. Cates, Étienne Fodor, Cesare Nardini, Julien Tailleur, and Frédéric van Wijland, “Statistical mechanics of active Ornstein-Uhlenbeck particles,” *Physical Review E* **103**, 032607 (2021).
 - [7] Dapeng Bi, Xingbo Yang, M. Cristina Marchetti, and M. Lisa Manning, “Motility-Driven Glass and Jamming Transitions in Biological Tissues,” *Physical Review X* **6**, 021011 (2016).
 - [8] Anshuman Pasupalak, Li Yan-Wei, Ran Ni, and Massimo Pica Ciamarra, “Hexatic phase in a model of active biological tissues,” *Soft Matter* **16**, 3914–3920 (2020).
 - [9] Meng-Yuan Li and Yan-Wei Li, “Relaxation dynamics in the self-propelled Voronoi model for epithelial monolayers,” *Physical Review Research* **6**, 033209 (2024).
 - [10] Emil Rozbicki, Manli Chuai, Antti I. Karjalainen, Feifei Song, Helen M. Sang, René Martin, Hans-Joachim Knölker, Michael P. MacDonald, and Cornelis J. Weijer, “Myosin-II-mediated cell shape changes and cell intercalation contribute to primitive streak formation,” *Nature Cell Biology* **17**, 397–408 (2015).
 - [11] Mehdi Saadaoui, Didier Rocancourt, Julian Roussel, Francis Corson, and Jerome Gros, “A tensile ring drives tissue flows to shape the gastrulating amniote embryo,” *Science* **367**, 453–458 (2020).
 - [12] Rastko Sknepnek, Ilyas Djafer-Cherif, Manli Chuai, Cornelis Weijer, and Silke Henkes, “Generating active T1 transitions through mechanochemical feedback,” *eLife* **12**, e79862 (2023).
 - [13] Fridtjof Brauns, Nikolas H. Claussen, Matthew F. Lefebvre, Eric F. Wieschaus, and Boris I. Shraiman, “The Geometric Basis of Epithelial Convergent Extension,” (2024), [bioRxiv:10.1101/2023.05.30.542935](https://doi.org/10.1101/2023.05.30.542935).
 - [14] Daisuke Mizuno, Catherine Tardin, C. F. Schmidt, and F. C. MacKintosh, “Nonequilibrium Mechanics of Active Cytoskeletal Networks,” *Science* **315**, 370–373 (2007).
 - [15] F. C. MacKintosh and A. J. Levine, “Nonequilibrium Mechanics and Dynamics of Motor-Activated Gels,” *Physical Review Letters* **100**, 018104 (2008).
 - [16] Frederick C MacKintosh and Christoph F Schmidt, “Active cellular materials,” *Current Opinion in Cell Biology* **22**, 29–35 (2010).
 - [17] Wim van Saarloos, Vincenzo Vitelli, and Zorana Zeravcic, *Soft Matter: Concepts, Phenomena, and Applications* (Princeton University Press, Princeton, 2024).
 - [18] Harukuni Ikeda, “Correlated noise and critical dimensions,” *Physical Review E* **108**, 064119 (2023).
 - [19] R. Maire and A. Plati, “Enhancing (quasi-)long-range order in a two-dimensional driven crystal,” (2024), [arXiv:2405.05621](https://arxiv.org/abs/2405.05621).
 - [20] Horst-Holger Boltz and Thomas Ihle, “Hyperuniformity in deterministic anti-aligning active matter,” (2024), [arXiv:2402.19451](https://arxiv.org/abs/2402.19451).
 - [21] Yuta Kuroda, Takeshi Kawasaki, and Kunimasa Miyazaki, “Long-range translational order and hyperuniformity in two-dimensional chiral active crystal,” (2024), [arXiv:2402.19192](https://arxiv.org/abs/2402.19192).
 - [22] Jianchao Chen, Xiaokang Lei, Yalun Xiang, Mengyuan Duan, Xingguang Peng, and H. P. Zhang, “Emergent Chirality and Hyperuniformity in an Active Mixture with Nonreciprocal Interactions,” *Physical Review Letters* **132**, 118301 (2024).
 - [23] Harukuni Ikeda and Yuta Kuroda, “Continuous symmetry breaking of low-dimensional systems driven by inhomogeneous oscillatory driving forces,” *Physical Review E* **110** (2024), [10.1103/physreve.110.024140](https://doi.org/10.1103/physreve.110.024140).
 - [24] Rainer Backofen, Abdelrahman Y. A. Altawil, Marco Salvalaglio, and Axel Voigt, “Nonequilibrium hyperuniform states in active turbulence,” *Proceedings of the National Academy of Sciences* **121** (2024), [10.1073/pnas.2320719121](https://doi.org/10.1073/pnas.2320719121).
 - [25] Yusheng Lei and Ran Ni, “Non-equilibrium dynamic hyperuniform states,” (2024), [arXiv:2405.12818](https://arxiv.org/abs/2405.12818).
 - [26] J. Prost, F. Jülicher, and J-F. Joanny, “Active gel physics,” *Nature Physics* **11**, 111–117 (2015).
 - [27] Amin Doostmohammadi, Jordi Ignés-Mullol, Julia M. Yeomans, and Francesc Sagués, “Active nematics,” *Nature Communications* **9**, 3246 (2018).
 - [28] Josep-Maria Armengol-Collado, Livio Nicola Carezza, Julia Eckert, Dimitrios Krommydas, and Luca Giomi, “Epithelia are multiscale active liquid crystals,” *Nature Physics* **19**, 1773–1779 (2023).
 - [29] Josep-Maria Armengol-Collado, Livio Nicola Carezza, and Luca Giomi, “Hydrodynamics and multiscale order in confluent epithelia,” *eLife* **13**, e86400 (2024).
 - [30] Xia-qing Shi, Fu Cheng, and Hugues Chaté, “Extreme Spontaneous Deformations of Active Crystals,” *Physical Review Letters* **131**, 108301 (2023).
 - [31] Bertrand I. Halperin, “On the Hohenberg–Mermin–Wagner Theorem and Its Limitations,” *Journal of Statistical Physics* **175**, 521–529 (2019).
 - [32] J M Kosterlitz, “Commentary on ‘Ordering, metastability and phase transitions in two-dimensional systems’ J M Kosterlitz and D J Thouless (1973 *J. Phys. C: Solid State Phys.* **6** 1181–203)—the early basis of the successful Kosterlitz–Thouless theory,” *Journal of Physics: Condensed Matter* **28**, 481001 (2016).
 - [33] Bernd Illing, Sebastian Fritschi, Herbert Kaiser, Christian L. Klix, Georg Maret, and Peter Keim, “Mermin–Wagner fluctuations in 2D amorphous solids,” *Proceedings of the National Academy of Sciences* **114**, 1856–1861 (2017).
 - [34] Brieuc Benvegnen, Omer Granek, Sunghan Ro, Ran Yaacoby, Hugues Chaté, Yariv Kafri, David Mukamel, Alexandre Solon, and Julien Tailleur, “Metastability of Discrete-Symmetry Flocks,” *Physical Review Letters* **131**, 218301 (2023).
 - [35] John Toner and Yuhai Tu, “Flocks, herds, and schools: A quantitative theory of flocking,” *Physical Review E* **58**, 4828–4858 (1998).
 - [36] Salvatore Torquato, “Hyperuniform states of matter,” *Physics Reports* **745**, 1–95 (2018).
 - [37] John Toner, Yuhai Tu, and Sriram Ramaswamy, “Hydrodynamics and phases of flocks,” *Annals of Physics* **318**, 170–244 (2005).
 - [38] Hugues Chaté, Francesco Ginelli, and Raúl Montagne, “Simple Model for Active Nematics: Quasi-Long-Range

- Order and Giant Fluctuations,” *Physical Review Letters* **96**, 180602 (2006).
- [39] Vijay Narayan, Sriram Ramaswamy, and Narayanan Menon, “Long-Lived Giant Number Fluctuations in a Swarming Granular Nematic,” *Science* **317**, 105–108 (2007).
- [40] Julien Deseigne, Olivier Dauchot, and Hugues Chaté, “Collective Motion of Vibrated Polar Disks,” *Physical Review Letters* **105**, 098001 (2010).
- [41] H. P. Zhang, Avraham Be’er, E.-L. Florin, and Harry L. Swinney, “Collective motion and density fluctuations in bacterial colonies,” *Proceedings of the National Academy of Sciences* **107**, 13626–13630 (2010).
- [42] Silke Henkes, Yaouen Fily, and M. Cristina Marchetti, “Active jamming: Self-propelled soft particles at high density,” *Physical Review E* **84**, 040301 (2011).
- [43] Leonardo Galliano, Michael E. Cates, and Ludovic Berthier, “Two-Dimensional Crystals far from Equilibrium,” *Physical Review Letters* **131**, 047101 (2023).
- [44] Salvatore Torquato and Frank H. Stillinger, “Local density fluctuations, hyperuniformity, and order metrics,” *Physical Review E* **68**, 041113 (2003).
- [45] Daniel Hexner and Dov Levine, “Noise, Diffusion, and Hyperuniformity,” *Physical Review Letters* **118**, 020601 (2017).
- [46] Filippo De Luca, Xiao Ma, Cesare Nardini, and Michael E. Cates, “Hyperuniformity in phase ordering: The roles of activity, noise, and non-constant mobility,” *Journal of Physics: Condensed Matter* **36**, 405101 (2024).
- [47] Alberto Fernandez-Nieves, Alexis De La Cotte, Daniel Pearce, Jyothishraj Nambisan, Aviv Levy, and Luca Giomi, “Hyperuniform Active Matter,” (2024), preprint.
- [48] Andrea Cavagna, Javier Cristin, Irene Giardina, and Mario Veca, “From noise on the sites to noise on the links: Discretizing the conserved Kardar-Parisi-Zhang equation in real space,” *Physical Review E* **109**, 064136 (2024).
- [49] Henri Peierls, “Quelques propriétés typiques des corps solides,” *Annales de l’Institut Henri Poincaré* **5**, 177–222 (1935).
- [50] David R. Nelson and B. I. Halperin, “Dislocation-mediated melting in two dimensions,” *Physical Review B* **19**, 2457–2484 (1979).
- [51] Mehran Kardar, *Statistical Physics of Fields*, 1st ed. (Cambridge University Press, 2007).
- [52] Michael Engel, Joshua A. Anderson, Sharon C. Glotzer, Masaharu Isobe, Etienne P. Bernard, and Werner Krauth, “Hard-disk equation of state: First-order liquid-hexatic transition in two dimensions with three simulation methods,” *Physical Review E* **87**, 042134 (2013).
- [53] Yan-Wei Li and Massimo Pica Ciamarra, “Accurate determination of the translational correlation function of two-dimensional solids,” *Physical Review E* **100**, 062606 (2019).
- [54] Kurt Binder and Walter Kob, *Glassy Materials and Disordered Solids: An Introduction to Their Statistical Mechanics* (World Scientific Publishing Company, 2005).
- [55] R. Kubo, “The fluctuation-dissipation theorem,” *Reports on Progress in Physics* **29**, 255 (1966).
- [56] M. Doi and S.F. Edwards, *The Theory of Polymer Dynamics*, International Series of Monographs on Physics (Oxford University Press, 1988).
- [57] Jana Tóthová and Vladimír Lisý, “Overdamped and underdamped Langevin equations in the interpretation of experiments and simulations,” *European Journal of Physics* **43**, 065103 (2022).
- [58] Reza Farhadifar, Jens-Christian Röper, Benoit Aigouy, Suzanne Eaton, and Frank Jülicher, “The Influence of Cell Mechanics, Cell-Cell Interactions, and Proliferation on Epithelial Packing,” *Current Biology* **17**, 2095–2104 (2007).
- [59] Alexander G. Fletcher, Miriam Osterfield, Ruth E. Baker, and Stanislav Y. Shvartsman, “Vertex Models of Epithelial Morphogenesis,” *Biophysical Journal* **106**, 2291–2304 (2014).
- [60] Daniel L. Barton, Silke Henkes, Cornelis J. Weijer, and Rastko Sknepnek, “Active Vertex Model for cell-resolution description of epithelial tissue mechanics,” *PLOS Computational Biology* **13**, e1005569 (2017).
- [61] Meryl A. Spencer, Zahera Jabeen, and David K. Lubensky, “Vertex stability and topological transitions in vertex models of foams and epithelia,” *The European Physical Journal E* **40**, 2 (2017).
- [62] Sijie Tong, Navreet K. Singh, Rastko Sknepnek, and Andrej Košmrlj, “Linear viscoelastic properties of the vertex model for epithelial tissues,” *PLOS Computational Biology* **18**, e1010135 (2022).
- [63] Shao-Zhen Lin, Matthias Merkel, and Jean-François Rupprecht, “Structure and Rheology in Vertex Models under Cell-Shape-Dependent Active Stresses,” *Physical Review Letters* **130**, 058202 (2023).
- [64] Scott Curran, Charlotte Strandkvist, Jasper Bathmann, Marc De Gennes, Alexandre Kabla, Guillaume Salbreux, and Buzz Baum, “Myosin II Controls Junction Fluctuations to Guide Epithelial Tissue Ordering,” *Developmental Cell* **43**, 480–492.e6 (2017).
- [65] Matej Krajnc, “Solid–fluid transition and cell sorting in epithelia with junctional tension fluctuations,” *Soft Matter* **16**, 3209–3215 (2020).
- [66] Charlie Duclut, Joris Paijmans, Mandar M. Inamdar, Carl D. Modes, and Frank Jülicher, “Nonlinear rheology of cellular networks,” *Cells & Development* **168**, 203746 (2021).
- [67] Takaki Yamamoto, Daniel M. Sussman, Tatsuo Shibata, and M. Lisa Manning, “Non-monotonic fluidization generated by fluctuating edge tensions in confluent tissues,” *Soft Matter* **18**, 2168–2175 (2022).
- [68] Yann-Edwin Keta and Silke Henkes, “github.com/yketa/cells,” GitHub repository, MIT license.
- [69] Yaouen Fily and M. Cristina Marchetti, “Athermal Phase Separation of Self-Propelled Particles with No Alignment,” *Physical Review Letters* **108**, 235702 (2012).
- [70] Rastko Sknepnek, Silke Henkes, Daniel Barton, and Amit Das, “github.com/sknepneklab/samos,” GitHub repository, GPL license.
- [71] G. Briand and O. Dauchot, “Crystallization of Self-Propelled Hard Discs,” *Physical Review Letters* **117**, 098004 (2016).
- [72] Walter Kob and Hans C. Andersen, “Testing mode-coupling theory for a supercooled binary Lennard-Jones mixture I: The van Hove correlation function,” *Physical Review E* **51**, 4626–4641 (1995).
- [73] Pasquale Digregorio, Demian Levis, Leticia F. Cugliandolo, Giuseppe Gonnella, and Ignacio Pagonabarraga, “Unified analysis of topological defects in 2D systems of active and passive disks,” *Soft Matter* **18**, 566–591 (2022).

- [74] Juliane U. Klamser, Sebastian C. Kapfer, and Werner Krauth, “Thermodynamic phases in two-dimensional active matter,” *Nature Communications* **9**, 5045 (2018).
- [75] Marc Durand and Julien Heu, “Thermally Driven Order-Disorder Transition in Two-Dimensional Soft Cellular Systems,” *Physical Review Letters* **123**, 188001 (2019).
- [76] N De Macedo Biniossek, H Löwen, Th Voigtmann, and F Smallegange, “Static structure of active Brownian hard disks,” *Journal of Physics: Condensed Matter* **30**, 074001 (2018).
- [77] Austin R. Dulaney, Stewart A. Mallory, and John F. Brady, “The “isothermal” compressibility of active matter,” *The Journal of Chemical Physics* **154**, 014902 (2021).
- [78] Sam Wilken, Aria Chaderjian, and Omar A. Saleh, “Spatial Organization of Phase-Separated DNA Droplets,” *Physical Review X* **13**, 031014 (2023).
- [79] Xinzhi Li, Amit Das, and Dapeng Bi, “Biological tissue-inspired tunable photonic fluid,” *Proceedings of the National Academy of Sciences* **115**, 6650–6655 (2018).
- [80] Yuanjian Zheng, Yan-Wei Li, and Massimo Pica Ciarrarra, “Hyperuniformity and density fluctuations at a rigidity transition in a model of biological tissues,” *Soft Matter* **16**, 5942–5950 (2020).
- [81] Yiwen Tang, Xinzhi Li, and Dapeng Bi, “Tunable Hyperuniformity in Cellular Structures,” (2024), [arXiv:2408.08976](https://arxiv.org/abs/2408.08976).
- [82] Yang Jiao, Hal Berman, Tim-Rasmus Kiehl, and Salvatore Torquato, “Spatial Organization and Correlations of Cell Nuclei in Brain Tumors,” *PLoS ONE* **6**, e27323 (2011).
- [83] Mingji Huang, Wensi Hu, Siyuan Yang, Quan-Xing Liu, and H. P. Zhang, “Circular swimming motility and disordered hyperuniform state in an algae system,” *Proceedings of the National Academy of Sciences* **118**, e2100493118 (2021).
- [84] Walter Kob and Hans C. Andersen, “Testing mode-coupling theory for a supercooled binary Lennard-Jones mixture. II. Intermediate scattering function and dynamic susceptibility,” *Physical Review E* **52**, 4134–4153 (1995).

Appendix A: Displacement fluctuations in a two-dimensional continuous medium

We consider the following equation of motion

$$\zeta \dot{\mathbf{u}}(\mathbf{r}, t) = - \int d^2 \mathbf{r}' \underline{\mathbf{D}}^{\text{el}}(\mathbf{r} - \mathbf{r}') \mathbf{u}(\mathbf{r}', t) + \boldsymbol{\lambda}(\mathbf{r}, t) \quad (\text{A1})$$

where $\mathbf{u}(\mathbf{r}, t)$ describes the elastic deformation from position \mathbf{r} , ζ is a friction coefficient, $\underline{\mathbf{D}}^{\text{el}}$ is a dynamical matrix [17] describing elasticity, and $\boldsymbol{\lambda}$ a stochastic term.

Using the Fourier transform in space and time of the displacement field

$$\mathbf{u}(\mathbf{r}, t) = \int d^2 \mathbf{q} e^{-i\mathbf{q}\cdot\mathbf{r}} \tilde{\mathbf{u}}(\mathbf{q}, t) = \int d^2 \mathbf{q} \int d\omega e^{-i\mathbf{q}\cdot\mathbf{r} - i\omega t} \tilde{\mathbf{U}}(\mathbf{q}, \omega), \quad (\text{A2})$$

we write (A1) in Fourier space

$$-i\omega\zeta\tilde{\mathbf{U}}(\mathbf{q}, \omega) = -\tilde{\underline{\mathbf{D}}}^{\text{el}}(\mathbf{q})\tilde{\mathbf{U}}(\mathbf{q}, \omega) - \tilde{\boldsymbol{\Lambda}}(\mathbf{q}, \omega). \quad (\text{A3})$$

We assume that the Fourier transform of the dynamical matrix $\tilde{\underline{\mathbf{D}}}^{\text{el}}(\mathbf{q})$ can be decomposed as follows [5]

$$\tilde{\underline{\mathbf{D}}}^{\text{el}}(\mathbf{q})\tilde{\mathbf{U}}(\mathbf{q}, \omega) = |\mathbf{q}|^2 \left[(B + \mu)\tilde{\mathbf{U}}_{\parallel}(\mathbf{q}, \omega) + \mu\tilde{\mathbf{U}}_{\perp}(\mathbf{q}, \omega) \right], \quad (\text{A4})$$

where $\hat{\mathbf{q}} = \mathbf{q}/|\mathbf{q}|$, $\tilde{\mathbf{U}}_{\parallel}(\mathbf{q}, \omega) = (\tilde{\mathbf{U}}(\mathbf{q}, \omega) \cdot \hat{\mathbf{q}})\hat{\mathbf{q}}$ and $\tilde{\mathbf{U}}_{\perp}(\mathbf{q}, \omega) = \tilde{\mathbf{U}}(\mathbf{q}, \omega) - \tilde{\mathbf{U}}_{\parallel}(\mathbf{q}, \omega)$ are respectively the longitudinal and transverse displacements in Fourier space, and B and μ are respectively the bulk and shear moduli. We can thus now write

$$\langle \tilde{\mathbf{U}}(\mathbf{q}, \omega) \cdot \tilde{\mathbf{U}}(\mathbf{q}', \omega')^* \rangle = \frac{\langle \tilde{\boldsymbol{\Lambda}}(\mathbf{q}, \omega) \cdot \tilde{\boldsymbol{\Lambda}}(\mathbf{q}', \omega')^* \rangle}{[-i\omega\zeta + |\mathbf{q}|^2(B + \mu)][i\omega'\zeta + |\mathbf{q}'|^2(B + \mu)]} + \frac{\langle \tilde{\boldsymbol{\Lambda}}(\mathbf{q}, \omega) \cdot \tilde{\boldsymbol{\Lambda}}(\mathbf{q}', \omega')^* \rangle}{[-i\omega\zeta + |\mathbf{q}|^2\mu][i\omega'\zeta + |\mathbf{q}'|^2\mu]} \quad (\text{A5})$$

We assume that the stochastic term is either the divergence of a tensor uncorrelated in space, or is a vector field uncorrelated in space, with correlations respectively

$$\langle \boldsymbol{\lambda}(\mathbf{r}, t) \cdot \boldsymbol{\lambda}(\mathbf{r}', t') \rangle = -\sigma^2 a^2 e^{-|t-t'|/\tau} \nabla^2 \delta(\mathbf{r} - \mathbf{r}'), \quad (\text{A6a})$$

$$\langle \boldsymbol{\lambda}(\mathbf{r}, t) \cdot \boldsymbol{\lambda}(\mathbf{r}', t') \rangle = f^2 a^2 e^{-|t-t'|/\tau} \delta(\mathbf{r} - \mathbf{r}'), \quad (\text{A6b})$$

where σ is an energy scale, f a force scale, a a coarse-graining length scale, and τ a persistence time. Using the following identity

$$\int dt \int dt' e^{-i(\omega t - \omega' t')} e^{-|t-t'|/\tau} = \frac{2\tau}{1 + \omega^2 \tau^2} \delta(\omega - \omega'), \quad (\text{A7})$$

we write these correlations in Fourier space

$$\langle \tilde{\boldsymbol{\Lambda}}(\mathbf{q}, \omega) \cdot \tilde{\boldsymbol{\Lambda}}(\mathbf{q}', \omega')^* \rangle = \frac{2\sigma^2 \tau |\mathbf{q}|^2}{1 + \omega^2 \tau^2} \delta(\omega - \omega') a^2 \delta(\mathbf{q} - \mathbf{q}'), \quad (\text{A8a})$$

$$\langle \tilde{\boldsymbol{\Lambda}}(\mathbf{q}, \omega) \cdot \tilde{\boldsymbol{\Lambda}}(\mathbf{q}', \omega')^* \rangle = \frac{2f^2 \tau}{1 + \omega^2 \tau^2} \delta(\omega - \omega') a^2 \delta(\mathbf{q} - \mathbf{q}'). \quad (\text{A8b})$$

We thus obtain the following space and time Fourier fluctuations

$$\langle \tilde{\mathbf{U}}(\mathbf{q}, \omega) \cdot \tilde{\mathbf{U}}(\mathbf{q}, \omega)^* \rangle = \frac{2\sigma^2 \tau |\mathbf{q}|^2 \delta(\omega - \omega') a^2 \delta(\mathbf{q} - \mathbf{q}')}{[\omega^2 \zeta^2 + |\mathbf{q}|^4 (B + \mu)^2][1 + \omega^2 \tau^2]} + \frac{2\sigma^2 \tau |\mathbf{q}|^2 \delta(\omega - \omega') a^2 \delta(\mathbf{q} - \mathbf{q}')}{[\omega^2 \zeta^2 + |\mathbf{q}|^4 \mu^2][1 + \omega^2 \tau^2]}, \quad (\text{A9a})$$

$$\langle \tilde{\mathbf{U}}(\mathbf{q}, \omega) \cdot \tilde{\mathbf{U}}(\mathbf{q}, \omega)^* \rangle = \frac{2g^2 \tau \delta(\omega - \omega') a^2 \delta(\mathbf{q} - \mathbf{q}')}{[\omega^2 \zeta^2 + |\mathbf{q}|^4 (B + \mu)^2][1 + \omega^2 \tau^2]} + \frac{2f^2 \tau \delta(\omega - \omega') a^2 \delta(\mathbf{q} - \mathbf{q}')}{[\omega^2 \zeta^2 + |\mathbf{q}|^4 \mu^2][1 + \omega^2 \tau^2]}. \quad (\text{A9b})$$

Using the following identities

$$\int_{-\infty}^{\infty} d\omega \frac{1}{a^2 + \omega^2 b^2} = \frac{\pi}{ab}, \quad (\text{A10a})$$

$$\begin{aligned} \int_{-\infty}^{\infty} d\omega \int_{-\infty}^{\infty} d\omega' e^{i(\omega - \omega')t} \frac{\delta(\omega - \omega')}{(a^2 + \omega^2 b^2)(c^2 + \omega^2 d^2)} &= \int_{-\infty}^{\infty} d\omega \frac{1}{b^2 c^2 - a^2 d^2} \left[\frac{b^2}{a^2 + \omega^2 b^2} - \frac{d^2}{c^2 + \omega^2 d^2} \right] \\ &= \frac{1}{b^2 c^2 - a^2 d^2} \left[\frac{\pi b}{a} - \frac{\pi d}{c} \right] \\ &= \frac{\pi}{ac[bc + ad]}, \end{aligned} \quad (\text{A10b})$$

we obtain the equal-time Fourier fluctuations

$$\langle \tilde{\mathbf{u}}(\mathbf{q}, t) \cdot \tilde{\mathbf{u}}(\mathbf{q}, t)^* \rangle = \frac{2\pi\sigma^2\tau|\mathbf{q}|^2 a^2 \delta(\mathbf{q} - \mathbf{q}')}{|\mathbf{q}|^2(B + \mu)[\zeta + |\mathbf{q}|^2(B + \mu)\tau]} + \frac{2\pi\sigma^2\tau|\mathbf{q}|^2 a^2 \delta(\mathbf{q} - \mathbf{q}')}{|\mathbf{q}|^2\mu[\zeta + |\mathbf{q}|^2\mu\tau]}, \quad (\text{A11a})$$

$$\langle \tilde{\mathbf{u}}(\mathbf{q}, t) \cdot \tilde{\mathbf{u}}(\mathbf{q}, t)^* \rangle = \frac{2\pi f^2\tau a^2 \delta(\mathbf{q} - \mathbf{q}')}{|\mathbf{q}|^2(B + \mu)[\zeta + |\mathbf{q}|^2(B + \mu)\tau]} + \frac{2\pi f^2\tau a^2 \delta(\mathbf{q} - \mathbf{q}')}{|\mathbf{q}|^2\mu[\zeta + |\mathbf{q}|^2\mu\tau]}, \quad (\text{A11b})$$

which correspond to (8) given the longitudinal and transversal correlation length scales $\xi_{\parallel} = \sqrt{(B + \mu)\tau/\zeta}$ and $\xi_{\perp} = \sqrt{\mu\tau/\zeta}$.

Appendix B: Displacement fluctuations in a two-dimensional triangular lattice

We consider a periodic triangular lattice in two dimensions, see Fig. B.1, where $\mathbf{e}_{\alpha} = a(\cos((\alpha - 1)\pi/3), \sin((\alpha - 1)\pi/3))$. We denote N the total number of sites – of the order of \sqrt{N} in each dimension –, \mathbf{r}_i^0 the reference lattice position of particle $i \in \{1, \dots, N\}$, and $\mathbf{u}_i = \mathbf{r}_i - \mathbf{r}_i^0$ its displacement from this lattice position. We define in this lattice the discrete divergence operator [48] which to a quantity $\mathbf{v}_{i \rightarrow \alpha}$ defined on links $i \rightarrow \alpha$ associates

$$\nabla \cdot \mathbf{v}_i = \sum_{\alpha=1}^3 [\mathbf{v}_{i \rightarrow \alpha} - \mathbf{v}_{(i-\alpha) \rightarrow \alpha}] \quad (\text{B1})$$

defined on sites i , and the Laplacian operator ∇^2 which to a quantity \mathbf{w}_i defined on sites i associates

$$\nabla^2 \mathbf{w}_i = \sum_{\alpha=1}^3 [\mathbf{w}_{i+\alpha} + \mathbf{w}_{i-\alpha} - 2\mathbf{w}_i] \quad (\text{B2})$$

also defined on sites i .

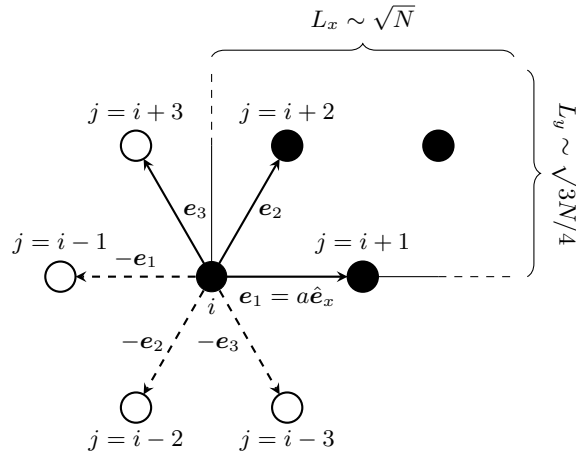


FIG. B.1. Notations within the triangular lattice.

We introduce the following overdamped equation of motion

$$\zeta \dot{\mathbf{u}}_i(t) - \gamma \nabla^2 \mathbf{u}_i = k \nabla^2 \mathbf{u}_i + \boldsymbol{\lambda}_i(t) \quad (\text{B3})$$

where ζ is a friction coefficient, γ a viscosity, k a spring constant, and $\boldsymbol{\lambda}_i(t)$ a stochastic term. We stress that given the dissipation term on the l.h.s. of (B3), the second fluctuation-dissipation theorem [55–57] dictates that the stochastic term $\boldsymbol{\lambda}_i(t)$ should have the following decomposition and correlations

$$\boldsymbol{\lambda}_i(t) = \boldsymbol{\eta}_i(t) + \nabla \cdot \boldsymbol{\sigma}_i, \quad (\text{B4a})$$

$$\langle \boldsymbol{\eta}_i(t) \cdot \boldsymbol{\eta}_j(t') \rangle = 2k_B T_1 \zeta \delta_{ij} \delta(t - t'), \quad (\text{B4b})$$

$$\langle \boldsymbol{\sigma}_{i \rightarrow \alpha}(t) \cdot \boldsymbol{\sigma}_{j \rightarrow \beta}(t') \rangle = 2k_B T_2 \gamma \delta_{ij} \delta_{\alpha\beta} \delta(t - t'), \quad (\text{B4c})$$

$$\langle \boldsymbol{\eta}_j(t) \cdot \boldsymbol{\sigma}_{j \rightarrow \beta}(t') \rangle = 0. \quad (\text{B4d})$$

with $T = T_1 = T_2$ the bath temperature.

We define the discrete space Fourier transform

$$\tilde{\mathbf{v}}_{\mathbf{q}} = \sum_{i=1}^N e^{-i\mathbf{q} \cdot \mathbf{r}_i^0} \mathbf{v}_i, \quad (\text{B5a})$$

$$\mathbf{v}_i = \frac{1}{N} \sum_{\substack{m,n=0 \\ \mathbf{q} = \frac{2\pi}{\sqrt{N}a}(m,n)}}^{N-1} e^{i\mathbf{q} \cdot \mathbf{r}_i^0} \tilde{\mathbf{v}}_{\mathbf{q}}, \quad (\text{B5b})$$

with the following orthogonality relation

$$\sum_{i=1}^N e^{-i(\mathbf{q}-\mathbf{q}') \cdot \mathbf{r}_i^0} = N \delta_{\mathbf{q},\mathbf{q}'}. \quad (\text{B6})$$

We write (B3) in Fourier space

$$-i\omega \zeta \tilde{\mathbf{U}}_{\mathbf{q}}(\omega) - i\omega Q(\mathbf{q})^2 \gamma \tilde{\mathbf{U}}_{\mathbf{q}}(\omega) = -Q(\mathbf{q})^2 k \tilde{\mathbf{U}}_{\mathbf{q}}(\omega) + \tilde{\boldsymbol{\Lambda}}_{\mathbf{q}}(\omega) \quad (\text{B7})$$

where we have introduced the kernel

$$Q(\mathbf{q})^2 = 2 \sum_{\alpha=1}^3 (1 - \cos(\mathbf{q} \cdot \mathbf{e}_{\alpha})) \Big|_{|\mathbf{q}| \rightarrow 0} \equiv \frac{3}{2} |\mathbf{q}|^2 a^2. \quad (\text{B8})$$

We thus obtain the following space and time Fourier fluctuations

$$\langle \tilde{\mathbf{U}}_{\mathbf{q}}(\omega) \cdot \tilde{\mathbf{U}}_{\mathbf{q}'}(\omega')^* \rangle = \frac{\langle \tilde{\boldsymbol{\Lambda}}_{\mathbf{q}}(\omega) \cdot \tilde{\boldsymbol{\Lambda}}_{\mathbf{q}'}(\omega')^* \rangle}{[-i\omega(\zeta + Q(\mathbf{q})^2 \gamma) + Q(\mathbf{q})^2 k][i\omega'(\zeta + Q(\mathbf{q}')^2 \gamma) + Q(\mathbf{q}')^2 k]}, \quad (\text{B9})$$

where the fluctuations of the driving noise derive from (B4)

$$\langle \tilde{\boldsymbol{\Lambda}}_{\mathbf{q}}(\omega) \cdot \tilde{\boldsymbol{\Lambda}}_{\mathbf{q}'}(\omega')^* \rangle = 2k_B T_1 \zeta N \delta_{\mathbf{q},\mathbf{q}'} \delta(\omega - \omega') + 2k_B T_2 \gamma Q(\mathbf{q})^2 N \delta_{\mathbf{q},\mathbf{q}'} \delta(\omega - \omega'). \quad (\text{B10})$$

We refine our expression of the displacement fluctuations

$$\langle \tilde{\mathbf{U}}_{\mathbf{q}}(\omega) \cdot \tilde{\mathbf{U}}_{\mathbf{q}'}(\omega')^* \rangle = \frac{2k_B T_1 \zeta N \delta_{\mathbf{q},\mathbf{q}'} \delta(\omega - \omega')}{\omega^2 (\zeta + Q(\mathbf{q})^2 \gamma)^2 + Q(\mathbf{q})^4 k^2} + \frac{2k_B T_2 \gamma Q(\mathbf{q})^2 N \delta_{\mathbf{q},\mathbf{q}'} \delta(\omega - \omega')}{\omega^2 (\zeta + Q(\mathbf{q})^2 \gamma)^2 + Q(\mathbf{q})^4 k^2}, \quad (\text{B11})$$

and take the inverse time Fourier transform using (A10) to compute the equal-time Fourier fluctuations

$$\langle \tilde{\mathbf{u}}_{\mathbf{q}}(t) \cdot \tilde{\mathbf{u}}_{\mathbf{q}'}(t)^* \rangle = \frac{2\pi k_B T_1 \zeta}{(\zeta + Q(\mathbf{q})^2 \gamma^2) Q(\mathbf{q})^2 k} N \delta_{\mathbf{q},\mathbf{q}'} + \frac{2\pi k_B T_2 \gamma}{(\zeta + Q(\mathbf{q})^2 \gamma^2) k} N \delta_{\mathbf{q},\mathbf{q}'}. \quad (\text{B12})$$

We stress here that $\langle |\tilde{\mathbf{u}}_{\mathbf{q}}(t)|^2 \rangle$ remains finite for $|\mathbf{q}| \rightarrow 0$ if and only if $T_1 = 0$ and $\zeta \neq 0$. Therefore, it is the competition between a fluctuating stress ($T_2 \neq 0$) and a particle-wise drag force ($\zeta \neq 0$) in the absence of a particle-wise fluctuating

force ($T_1 = 0$) which damps large-wavelength fluctuations. Moreover, the effect of an additional viscosity-like term only affects the small-wavelength behaviour.

We acknowledge that a similar derivation was performed in Ref. [19].

We provide the derivation for a fluctuating stress with finite-time correlations

$$\boldsymbol{\lambda}_i(t) = \nabla \cdot \boldsymbol{\sigma}_i, \quad (\text{B13a})$$

$$\langle \boldsymbol{\sigma}_{i \rightarrow \alpha}(t) \cdot \boldsymbol{\sigma}_{j \rightarrow \beta}(t') \rangle = \sigma^2 a^{-2} e^{-|t-t'|/\tau} \delta_{ij} \delta_{\alpha\beta} \delta(t-t'), \quad (\text{B13b})$$

which read in Fourier space

$$\langle \tilde{\boldsymbol{\Lambda}}_{\mathbf{q}}(\omega) \cdot \tilde{\boldsymbol{\Lambda}}_{\mathbf{q}'}(\omega')^* \rangle = \frac{2\sigma^2 a^{-2} \tau Q(\mathbf{q})^2}{1 + \omega^2 \tau^2} N \delta_{\mathbf{q}, \mathbf{q}'} \delta(\omega - \omega'). \quad (\text{B14})$$

such that the space and time Fourier fluctuations are

$$\langle \tilde{\mathbf{U}}_{\mathbf{q}}(\omega) \cdot \tilde{\mathbf{U}}_{\mathbf{q}'}(\omega')^* \rangle = \frac{2\sigma^2 a^{-2} \tau}{[\omega^2 \zeta^2 + Q(\mathbf{q})^4 k^2][1 + \omega^2 \tau^2]} N \delta_{\mathbf{q}, \mathbf{q}'} \delta(\omega - \omega'). \quad (\text{B15})$$

We use (A10) and write the equal-time Fourier fluctuations

$$\langle \tilde{\mathbf{u}}_{\mathbf{q}}(t) \cdot \tilde{\mathbf{u}}_{\mathbf{q}'}(t)^* \rangle = \frac{2\pi\sigma^2 a^{-2} \tau}{k(\zeta + Q(\mathbf{q})^2 k \tau)} N \delta_{\mathbf{q}, \mathbf{q}'} = \frac{2\pi\sigma^2 \tau^2}{\zeta^2} \frac{\xi^{-2}}{1 + Q(\mathbf{q})^2 (\xi/a)^2} N \delta_{\mathbf{q}, \mathbf{q}'}, \quad (\text{B16})$$

where we have introduced the correlation length $\xi = a\sqrt{k\tau/\zeta}$. We obtain the same large-wavelength scaling as (B12): the finite-time correlation of the stress only affects the small-wavelength fluctuations.

Appendix C: Large-distance scaling of the translational order correlation function

We consider the local translational order parameter

$$\psi_{\mathbf{q}_0, i} = e^{i\mathbf{q}_0 \cdot (\mathbf{r}_i - \mathbf{r}_0)} \quad (\text{C1})$$

where \mathbf{q}_0 is a reciprocal vector of the lattice, $\mathbf{r}_i = \mathbf{r}_i^0 + \mathbf{u}_i$ the position of particle i which is displaced of \mathbf{u}_i from its lattice position \mathbf{r}_i^0 . We write the fluctuations

$$\langle \psi_{\mathbf{q}_0, i} \psi_{\mathbf{q}_0, j}^* \rangle = \langle e^{i\mathbf{q}_0 \cdot (\mathbf{r}_j - \mathbf{r}_i)} \rangle = \langle e^{i\mathbf{q}_0 \cdot (\mathbf{r}_j^0 - \mathbf{r}_i^0)} e^{i\mathbf{q}_0 \cdot (\mathbf{u}_j - \mathbf{u}_i)} \rangle. \quad (\text{C2})$$

We note that for two lattice points \mathbf{r}_i^0 and \mathbf{r}_j^0 then $\mathbf{q}_0 \cdot (\mathbf{r}_j^0 - \mathbf{r}_i^0)$ is 0 modulo 2π therefore $e^{i\mathbf{q}_0 \cdot (\mathbf{r}_j^0 - \mathbf{r}_i^0)} = 1$. We also define for a random variable X its characteristic function $t \mapsto \langle \exp(itX) \rangle$. For a normally distributed random variable X with zero mean $\langle X \rangle = 0$ then

$$\langle \exp(itX) \rangle = \exp\left(-\frac{1}{2}t^2 \langle X^2 \rangle\right). \quad (\text{C3})$$

We assume for two distant particles i and j that $\mathbf{q}_0 \cdot (\mathbf{r}_j - \mathbf{r}_i)$ is normally distributed – from the linearity of (B3) the Gaussian nature of driving noises – and assume from isotropy

$$\langle (\mathbf{q}_0 \cdot (\mathbf{u}_j - \mathbf{u}_i))^2 \rangle = \frac{1}{2} |\mathbf{q}_0|^2 \langle |\mathbf{u}_j - \mathbf{u}_i|^2 \rangle = |\mathbf{q}_0|^2 \langle |\mathbf{u}_i|^2 \rangle - |\mathbf{q}_0|^2 \langle \mathbf{u}_i \cdot \mathbf{u}_j \rangle \quad (\text{C4})$$

where we have used $\langle |\mathbf{u}_i|^2 \rangle = \langle |\mathbf{u}_j|^2 \rangle$ for all i in steady state.

As a matter of simplification we use the continuous-space spectrum of displacements (8) to compute the correlations $\langle |\mathbf{u}_i|^2 \rangle$ and $\langle \mathbf{u}_i \cdot \mathbf{u}_j \rangle$. We then write

$$\langle |\mathbf{u}_i|^2 \rangle = \int d^2 \mathbf{q} \int d^2 \mathbf{q}' \langle \tilde{\mathbf{u}}(\mathbf{q}, t) \cdot \tilde{\mathbf{u}}(\mathbf{q}', t)^* \rangle, \quad (\text{C5a})$$

$$\langle \mathbf{u}_i \cdot \mathbf{u}_j \rangle = \langle \mathbf{u}_j \cdot \mathbf{u}_i \rangle = \int d^2 \mathbf{q} \int d^2 \mathbf{q}' \cos(\mathbf{q} \cdot \mathbf{r}_j^0 - \mathbf{q}' \cdot \mathbf{r}_i^0) \langle \tilde{\mathbf{u}}(\mathbf{q}, t) \cdot \tilde{\mathbf{u}}(\mathbf{q}', t)^* \rangle. \quad (\text{C5b})$$

such that using (C4)

$$\langle (\mathbf{q}_0 \cdot (\mathbf{u}_j - \mathbf{u}_i))^2 \rangle = |\mathbf{q}_0|^2 \int d^2\mathbf{q} \int d^2\mathbf{q}' [1 - \cos(\mathbf{q} \cdot \mathbf{r}_j^0 - \mathbf{q} \cdot \mathbf{r}_i^0)] \langle \tilde{\mathbf{u}}(\mathbf{q}, t) \cdot \tilde{\mathbf{u}}(\mathbf{q}', t)^* \rangle. \quad (\text{C6})$$

We note that (8) are symmetric by rotation of \mathbf{q} . With

$$\Delta = \mathbf{r}_j^0 - \mathbf{r}_i^0, \quad r = |\Delta|, \quad (\text{C7})$$

we define for all wave vector \mathbf{q} the angle ϕ such that $\mathbf{q} \cdot \Delta = qr \cos \phi$ where $q = |\mathbf{q}|$. Therefore for any function $f(|\mathbf{q}|)$ we have the following identity

$$\int d^2\mathbf{q} \cos(\mathbf{q} \cdot \Delta) f(|\mathbf{q}|) = \int dq \int_0^{2\pi} d\phi q \cos(qr \cos \phi) f(q) = \int dq 2\pi q J_0(qr) f(q), \quad (\text{C8a})$$

$$\int d^2\mathbf{q} f(|\mathbf{q}|) = \int dq 2\pi q f(q), \quad (\text{C8b})$$

where J_0 is the 0-th Bessel function of the first kind.

C.1. Fluctuating stress

Using (8a), (C6), and (C8), we write

$$\langle |\mathbf{u}_i|^2 \rangle = \frac{(2\pi)^2 \sigma^2 \tau^2 a^2}{\zeta^2} \left[\int_{2\pi/L}^{2\pi/a} dq \frac{q}{\xi_{\parallel}^2 (1 + q^2 \xi_{\parallel}^2)} + \int_{2\pi/L}^{2\pi/a} dq \frac{q}{\xi_{\perp}^2 (1 + q^2 \xi_{\perp}^2)} \right], \quad (\text{C9a})$$

$$\langle \mathbf{u}_i \cdot \mathbf{u}_j \rangle = \frac{(2\pi)^2 \sigma^2 \tau^2 a^2}{\zeta^2} \left[\int_{2\pi/L}^{2\pi/a} dq \frac{q J_0(qr)}{\xi_{\parallel}^2 (1 + q^2 \xi_{\parallel}^2)} + \int_{2\pi/L}^{2\pi/a} dq \frac{q J_0(qr)}{\xi_{\perp}^2 (1 + q^2 \xi_{\perp}^2)} \right], \quad (\text{C9b})$$

where the upper cutoff in the integral translates the fact that the continuous description applies to scales greater than the coarse-graining scale a , and the lower cutoff corresponds to the system size. At fixed r both integrals converge for $L \rightarrow \infty$, we thus take this limit for the derivation below. To compute (C9a) we use the following identity

$$\int_0^{2\pi/a} dq \frac{q}{1 + q^2 \xi^2} = \frac{1}{2\xi^2} \log \left(1 + (2\pi)^2 \frac{\xi^2}{a^2} \right) \quad (\text{C10})$$

and write

$$\langle |\mathbf{u}_i|^2 \rangle \Big|_{L \rightarrow \infty} = \frac{(2\pi)^2 \sigma^2 \tau^2 a^2}{2\zeta^2} \left[\frac{1}{\xi_{\parallel}^4} \log \left(1 + (2\pi)^2 (\xi_{\parallel}/a)^2 \right) + \frac{1}{\xi_{\perp}^4} \log \left(1 + (2\pi)^2 (\xi_{\perp}/a)^2 \right) \right] \equiv \langle u^2 \rangle_{\infty}. \quad (\text{C11})$$

To compute (C9b) we use the following inequality

$$|J_0(qr)| \leq \frac{1}{\sqrt{qr}} \quad (\text{C12})$$

to bound the following integral

$$\left| \int_0^{2\pi/a} dq \frac{q J_0(qr)}{1 + q^2 \xi^2} \right| \leq \frac{1}{\sqrt{r}} \int_0^{2\pi/a} dq \frac{\sqrt{q}}{1 + q^2 \xi^2} \xrightarrow{r \rightarrow \infty} 0 \quad (\text{C13})$$

where the latter limit derives from the fact that the integral is finite, which implies

$$\langle \mathbf{u}_i \cdot \mathbf{u}_j \rangle \xrightarrow[\substack{L \rightarrow \infty \\ r \rightarrow \infty}]{} 0. \quad (\text{C14})$$

Therefore, using (C2), (C3), (C4), (C11), and (C14), we obtain

$$\langle \psi_{\mathbf{q}_0, i} \psi_{\mathbf{q}_0, j}^* \rangle \Big|_{\substack{L \rightarrow \infty \\ |\mathbf{r}_j^0 - \mathbf{r}_i^0| \rightarrow \infty}} = \exp \left(-\frac{1}{2} |\mathbf{q}_0|^2 \langle u^2 \rangle_{\infty} \right). \quad (\text{C15})$$

C.2. Fluctuating force

Using (8b), (C6), and (C8), we write

$$\langle |\mathbf{u}_i|^2 \rangle = \frac{(2\pi)^2 f^2 \tau^2 a^2}{\zeta^2} \left[\int_{2\pi/L}^{2\pi/a} dq \frac{q}{q^2 \xi_{\parallel}^2 (1 + q^2 \xi_{\parallel}^2)} + \int_{2\pi/L}^{2\pi/a} dq \frac{q}{q^2 \xi_{\perp}^2 (1 + q^2 \xi_{\perp}^2)} \right], \quad (\text{C16a})$$

$$\langle (\mathbf{q}_0 \cdot (\mathbf{u}_j - \mathbf{u}_i))^2 \rangle = \frac{(2\pi)^2 f^2 \tau^2 a^2 |\mathbf{q}_0|^2}{\zeta^2} \left[\int_{2\pi/L}^{2\pi/a} dq \frac{q(1 - J_0(qr))}{q^2 \xi_{\parallel}^2 (1 + q^2 \xi_{\parallel}^2)} + \int_{2\pi/L}^{2\pi/a} dq \frac{q(1 - J_0(qr))}{q^2 \xi_{\perp}^2 (1 + q^2 \xi_{\perp}^2)} \right], \quad (\text{C16b})$$

where the upper cutoff in the integral translates the fact that the continuous description applies to scales greater than the coarse-graining scale a , and the lower cutoff corresponds to the system size. To compute (C16a) we note that $q[q^2(1 + q^2 \xi^2)]^{-1} \sim q^{-1}$ for $q \rightarrow 0$ and $\int_{2\pi/L}^{2\pi/a} dq q^{-1}$ diverges for $L \rightarrow \infty$, therefore we can use the equivalence of the integrals

$$\int_{2\pi/L}^{2\pi/a} dq \frac{q}{q^2(1 + q^2 \xi^2)} \stackrel{L \rightarrow \infty}{=} \int_{2\pi/L}^{2\pi/a} dq \frac{1}{q} = \log(L/a), \quad (\text{C17})$$

and write

$$\langle |\mathbf{u}_i|^2 \rangle \stackrel{L \rightarrow \infty}{=} \frac{(2\pi)^2 \sigma^2 \tau^2 a^2}{\zeta^2} \left[\frac{1}{\xi_{\parallel}^2} + \frac{1}{\xi_{\perp}^2} \right] \log(L/a) \equiv C \log(L/a). \quad (\text{C18})$$

To compute (C16b) we first note that at fixed r both integrals converge for $L \rightarrow \infty$, we thus take this limit for the derivation below. We focus on the following integral

$$\int_0^{2\pi/a} dq \frac{q(1 - J_0(qr))}{q^2(1 + q^2 \xi^2)} = \int_0^{2\pi/r} dq \frac{q(1 - J_0(qr))}{q^2(1 + q^2 \xi^2)} + \int_{2\pi/r}^{2\pi/a} dq \frac{q}{q^2(1 + q^2 \xi^2)} - \int_{2\pi/r}^{2\pi/a} dq \frac{q J_0(qr)}{q^2(1 + q^2 \xi^2)}. \quad (\text{C19})$$

This decomposition is such that the first term on the r.h.s. cancels in the limit $r \rightarrow \infty$. For the second term we note once again that $q[q^2(1 + q^2 \xi^2)]^{-1} \sim q^{-1}$ for $q \rightarrow 0$ and $\int_{2\pi/r}^{2\pi/a} dq q^{-1}$ diverges for $r \rightarrow \infty$, therefore we can use the equivalence on the integrals

$$\int_{2\pi/r}^{2\pi/a} dq \frac{q}{q^2(1 + q^2 \xi^2)} \stackrel{r \rightarrow \infty}{=} \int_{2\pi/r}^{2\pi/a} dq \frac{1}{q} = \log(r/a). \quad (\text{C20})$$

Finally for the third term, using (C12) we bound the integral in the following way

$$\left| \int_{2\pi/r}^{2\pi/a} dq \frac{q J_0(qr)}{q^2(1 + q^2 \xi^2)} \right| \leq \frac{1}{\sqrt{r}} \int_{2\pi/r}^{2\pi/a} dq \frac{1}{q^{3/2}(1 + q^2 \xi^2)}, \quad (\text{C21})$$

where we note once again that $[q^{3/2}(1 + q^2 \xi^2)]^{-1} \sim q^{-3/2}$ for $q \rightarrow 0$ and $\int_{2\pi/r}^{2\pi/a} dq q^{-3/2}$ diverges for $r \rightarrow \infty$, therefore we can use the equivalence on the integrals

$$\frac{1}{\sqrt{r}} \int_{2\pi/r}^{2\pi/a} dq \frac{1}{q^{3/2}(1 + q^2 \xi^2)} \stackrel{r \rightarrow \infty}{=} \frac{1}{\sqrt{r}} \int_{2\pi/r}^{2\pi/a} dq \frac{1}{q^{3/2}} = \frac{1}{\sqrt{2\pi}} \left[1 - \sqrt{\frac{a}{r}} \right], \quad (\text{C22})$$

which is finite in the $r \rightarrow \infty$ limit. Therefore only the second term in the r.h.s. of (C19) diverges, and we have the following equivalence

$$\int_0^{2\pi/a} dq \frac{q(1 - J_0(qr))}{q^2(1 + q^2 \xi^2)} \stackrel{r \rightarrow \infty}{=} \log(r/a). \quad (\text{C23})$$

which eventually leads to

$$\langle (\mathbf{q}_0 \cdot (\mathbf{u}_j - \mathbf{u}_i))^2 \rangle \stackrel{L \rightarrow \infty}{=} \frac{(2\pi)^2 f^2 \tau^2 a^2 |\mathbf{q}_0|^2}{\zeta^2} \left[\frac{1}{\xi_{\parallel}^2} + \frac{1}{\xi_{\perp}^2} \right] \log(r/a) = |\mathbf{q}_0|^2 C \log(r/a). \quad (\text{C24})$$

Therefore, using (C2), (C3), (C18), and (C24), we obtain

$$\langle \psi_{\mathbf{q}_0, i} \psi_{\mathbf{q}_0, j}^* \rangle \stackrel{L \rightarrow \infty}{=} (r/a)^{-\frac{1}{2}} |\mathbf{q}_0|^2 C. \quad (\text{C25})$$

Appendix D: Large-wavelength scaling of the structure factor

We consider the structure factor

$$S(\mathbf{q}) = \frac{1}{N} \sum_{i,j=1}^N \langle e^{-i\mathbf{q}\cdot(\mathbf{r}_j - \mathbf{r}_i)} \rangle = \frac{1}{N} \sum_{i,j=1}^N e^{-i\mathbf{q}\cdot(\mathbf{r}_j^0 - \mathbf{r}_i^0)} \langle e^{-i\mathbf{q}\cdot(\mathbf{u}_j - \mathbf{u}_i)} \rangle. \quad (\text{D1})$$

For normally distributed driving noise then, due to the linearity of (19), displacements are also normally distributed. Using (C3) we write

$$\langle \exp(-i\mathbf{q}\cdot(\mathbf{u}_j - \mathbf{u}_i)) \rangle = \exp\left(-\frac{1}{2}\langle(\mathbf{q}\cdot(\mathbf{u}_j - \mathbf{u}_i))^2\rangle\right) = \exp\left(-\frac{1}{4}|\mathbf{q}|^2\langle|\mathbf{u}_j - \mathbf{u}_i|^2\rangle\right) \quad (\text{D2})$$

where the second equality derives from isotropy. It is possible to Taylor expand the latter exponential if

$$|\mathbf{q}|^2\langle|\mathbf{u}_j - \mathbf{u}_i|^2\rangle \ll 1. \quad (\text{D3})$$

In the limit $L \rightarrow \infty$ we consider wavevectors such that

$$|\mathbf{q}| \sim \frac{2\pi}{L}. \quad (\text{D4})$$

Therefore, considering $\langle|\mathbf{u}_i - \mathbf{u}_j|^2\rangle \leq 2\langle|\mathbf{u}_i|^2\rangle$ in steady state, and the following scalings

$$\langle|\mathbf{u}_i|^2\rangle \underset{L \rightarrow \infty}{=} \langle u^2 \rangle_\infty, \quad (\text{D5a})$$

$$\langle|\mathbf{u}_i|^2\rangle \underset{L \rightarrow \infty}{=} C \log(L/a), \quad (\text{D5b})$$

for fluctuating stress (C11) and fluctuating force (C18) respectively, we have that condition (D3) is satisfied for large enough $L \gg a$. We then write

$$\begin{aligned} S(\mathbf{q}) &\underset{\substack{L \rightarrow \infty \\ |\mathbf{q}| \sim 2\pi/L}}{=} \frac{1}{N} \sum_{i,j=1}^N e^{-i\mathbf{q}\cdot(\mathbf{r}_j^0 - \mathbf{r}_i^0)} \left(1 - \frac{1}{4}|\mathbf{q}|^2\langle|\mathbf{u}_j - \mathbf{u}_i|^2\rangle\right) \\ &= \frac{1}{N} \sum_{i,j=1}^N e^{-i\mathbf{q}\cdot(\mathbf{r}_j^0 - \mathbf{r}_i^0)} \left(1 - \frac{1}{2}|\mathbf{q}|^2\langle|\mathbf{u}_i|^2\rangle + \frac{1}{2}|\mathbf{q}|^2\langle\mathbf{u}_i \cdot \mathbf{u}_j\rangle\right), \end{aligned} \quad (\text{D6})$$

where the first two terms cancel due to the orthogonality relation (B6). Using (B5) we thus obtain

$$S(\mathbf{q}) \underset{\substack{L \rightarrow \infty \\ |\mathbf{q}| \sim 2\pi/L}}{=} \frac{1}{2N} |\mathbf{q}|^2 \langle|\tilde{\mathbf{u}}_{\mathbf{q}}|^2\rangle. \quad (\text{D7})$$

Appendix E: Dynamical transition in active Brownian particles (ABP) and pair active Brownian particles (pABP)

We analyse the melting transition in both our particle models – active Brownian particles (ABP) and pair active Brownian particles (pABP) – from a dynamical point of view, using two-time correlation functions borrowed from glass physics. First, the mean square displacement $\text{MSD}(t)$ (27) [72] which corresponds to the variance of displacements over particles as a function of time, and the self-intermediate scattering function [84]

$$F_s(\mathbf{k}, t) = \left\langle \left| \frac{1}{N} \sum_{i=1}^N \exp(\mathbf{i}\mathbf{k} \cdot ([\mathbf{r}_i(t) - \bar{\mathbf{r}}(t)] - [\mathbf{r}_i(0) - \bar{\mathbf{r}}(0)])) \right|^2 \right\rangle, \quad (\text{E1})$$

with $\bar{\mathbf{r}}(t) = (1/N) \sum_{i=1}^N \mathbf{r}_i(t)$ the position of the centre of mass at time t and $\mathbf{k} = 2\pi(1/D, 0)$, which may be interpreted as the proportion of particles whose displacements at time t are less than $2\pi/|\mathbf{k}| = D$ in norm, assuming isotropy. We show both functions in Fig. E.1.

In the ABP model, the melting transition of the soft crystal lies between $f = 0.07$ and 0.08 , with a bounded MSD (Fig. E.1(a)) and no or few defects below that value, and a defect-rich liquid above that value. Melting is also evident in the more rapid decay of the self-intermediate scattering function above the transition (Fig. E.1(c)).

In the pABP model, there is an abrupt transition from solid to liquid between $f = 0.11$ and 0.117 , evident in the change between a state with very low plateau values of the MSD (Fig. E.1(b)) and a correspondingly high plateau value of the self-intermediate scattering function (Fig. E.1(d)) on the one hand, and a rapidly diffusing liquid state where correlations are lost on the other hand.

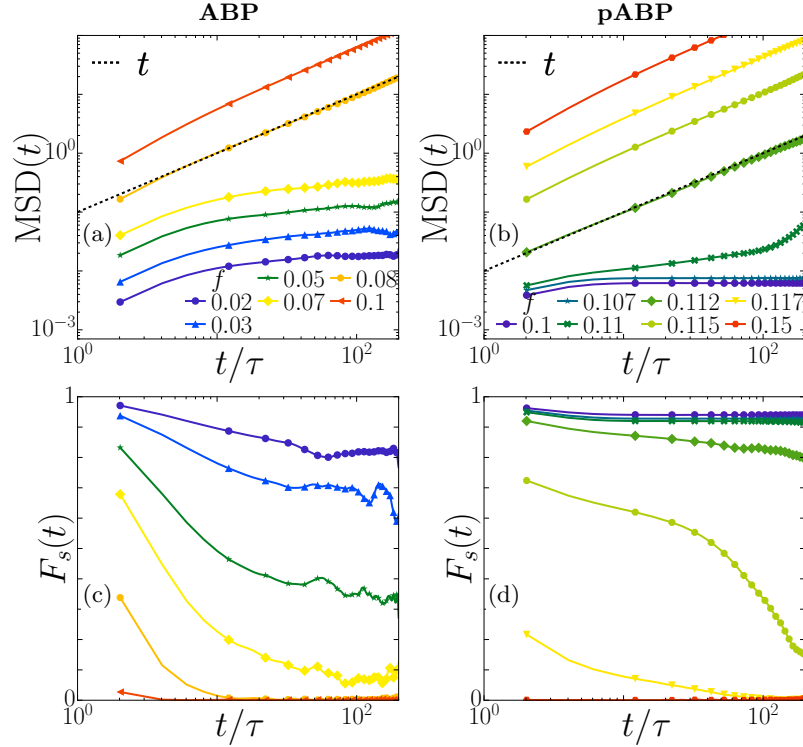


FIG. E.1. (a, b) Mean squared displacements as functions of time $\text{MSD}(t)$ (27) in steady state for different stochastic force amplitudes f . Dashed lines are linear functions of time as guides to the eye. (c, d) Self-intermediate scattering function $F_s(t)$ (E1) in steady state for different stochastic force amplitudes f . (a, c) Active Brownian particles (ABP) and (b, d) pair active Brownian particles (pABP), with $N = 16384$ particles and persistence time $\tau_p = 25$. Identical markers between (a) and (c) and between (b) and (d) correspond to identical data sets.

Appendix F: Phase coexistence in pair active Brownian particles (pABP)

We illustrate the dynamical aspect of the phase-separated configuration of the pair active Brownian particle model at $f = 0.115$ (Fig. 3(c, d)) with a time-lapse of this system (Fig. F.1). We highlight structural order with three descriptors: the local orientational order parameter $\psi_{6,i}$ (11) (Fig. F.1(a-c)) which characterises the local orientation of the lattice, the local translational order parameter $\psi_{q_0,i}$ (Fig. F.1(d-f)) which characterises the translational regularity of the lattice, and the coordination z_i of particles (Fig. F.1(g-i)), *i.e.* the number of neighbours of each particle. We compute these neighbours with a Delaunay triangulation from the particles' positions. We stress that in a regular triangular lattice, $z_i = 6$. Coordination numbers $z_i \neq 6$ (typically $z_i = 5$ or 7) characterise topological defects known as *disclinations* which locally break translational order. However orientational order is not broken if these defects are bound. In this latter case they correspond to a *dislocation*.

Fig. F.1 shows that the molten state slowly nucleates (over times much larger than τ) from the crystalline state, a scenario reminiscent of first-order transitions.

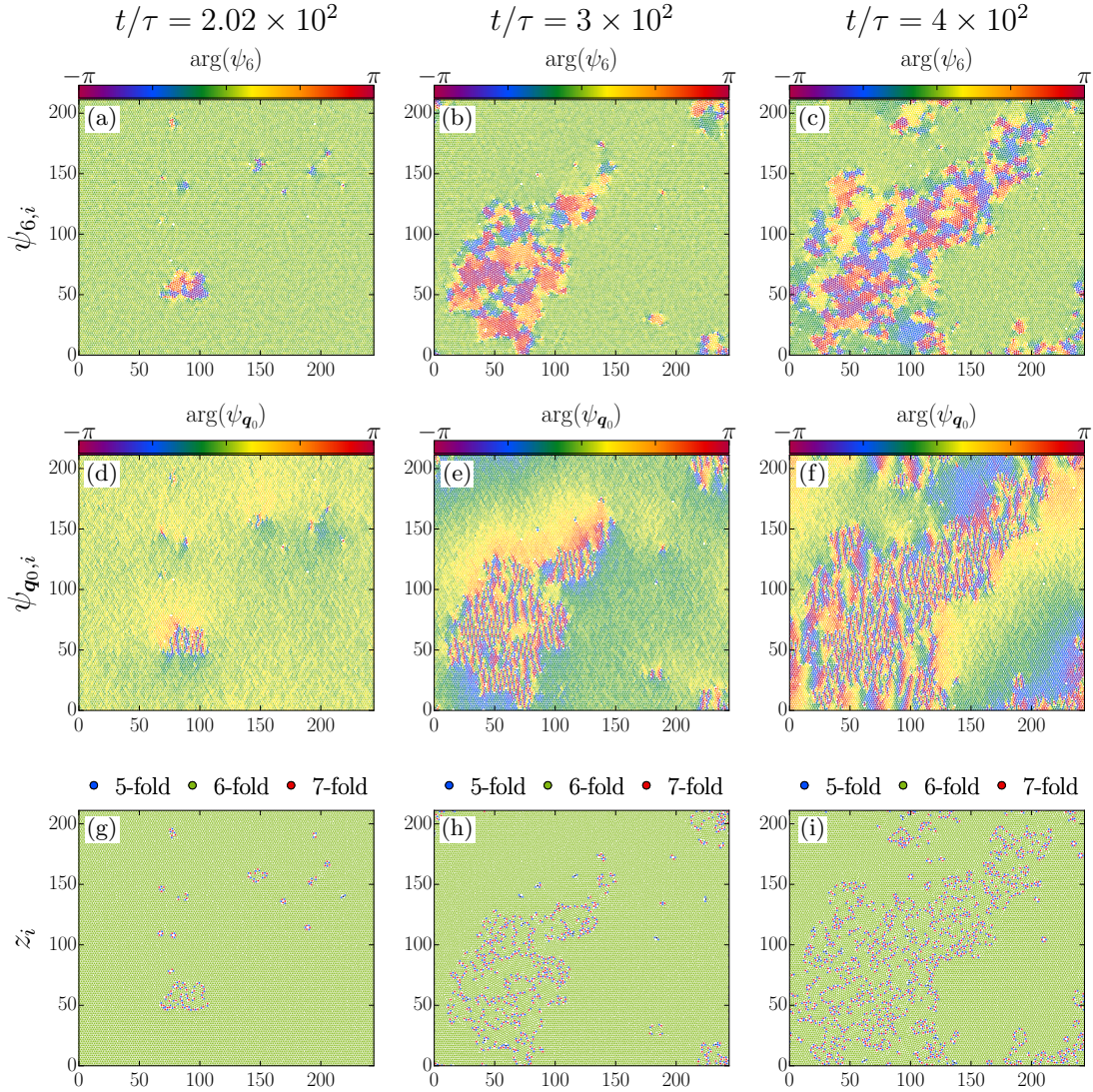


FIG. F.1. Time lapse of order in a system of pair active Brownian particles (pABP) at $f = 0.115$ with $N = 16384$ particles and persistence time $\tau = 25$: (a, d, g) $t = 5.05 \times 10^3$ *i.e.* $t/\tau = 2.02 \times 10^2$, (b, e, h) $t = 7.5 \times 10^3$ *i.e.* $t/\tau = 3 \times 10^2$, and (c, f, i) $t = 1 \times 10^4$ *i.e.* $t/\tau = 4 \times 10^2$. We visualise (a-c) the argument of the local hexatic order parameter $\arg(\psi_{6,i})$ (11) (see Fig. 3(g) for a correspondence to the local orientation), (d-f) the argument of the local translational order parameter $\arg(\psi_{q_0,i})$ (12), and (g-i) the coordination number z_i of particles. In this representation, particles with coordination numbers $z_i \neq 5, 6, 7$ are represented in black.

Appendix G: Defects in pair active Brownian particles (pABP)

We reproduce in Fig. G.1(a-f) the snapshots of Fig. 3 and add the corresponding visualisation of the coordination number z_i of particles (Fig. G.1(g-i), see definition in Appendix F).

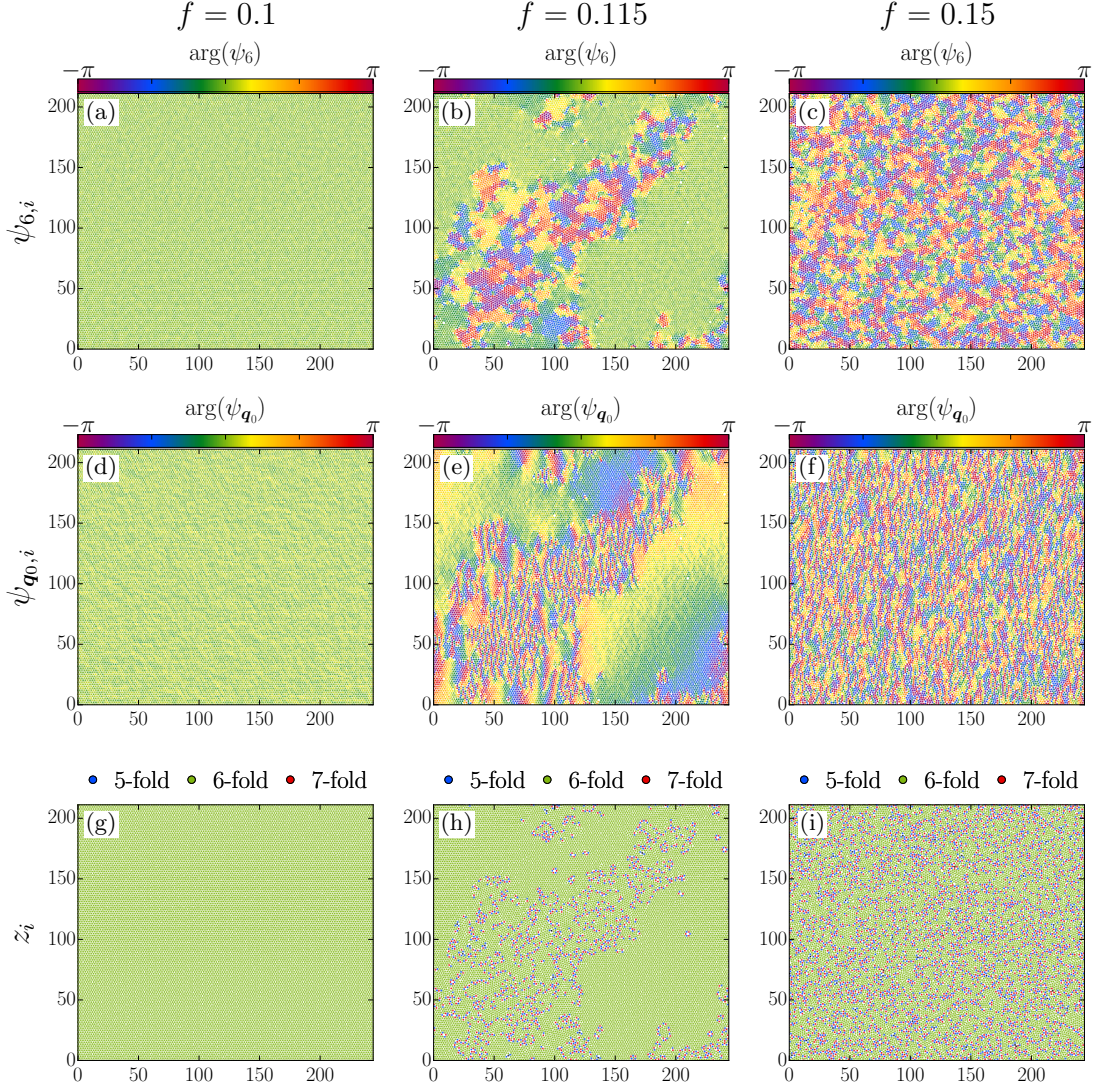


FIG. G.1. Order and disorder for pair active Brownian particles (pABP). Visualisation of the argument of the local hexatic order parameter $\arg(\psi_{6,i})$ (11) (a-c), the argument of the local translational order parameter $\arg(\psi_{q_0,i})$ (12) (d-f), and the coordination number z_i of particles (g-i). We used $N = 16384$ particles and persistence time $\tau = 25$. Stochastic force amplitude is (a, d, g) $f = 0.1$, (b, e, h) $f = 0.115$, (c, f, i) $f = 0.15$.

Appendix H: Structural transition in active Brownian particles (ABP) and pair active Brownian particles (pABP)

We analyse the melting transition in both our particle models – active Brownian particles (ABP) and pair active Brownian particles (pABP) – from a structural point of view, using on the one hand the global orientational order parameter Ψ_6 and global translational order parameter Ψ_{q_0} (13), and on the other hand the spatial decay of the orientational order correlation function $C_6(r)$ and translational order correlation function $C_{q_0}(r)$ (14).

In both models, liquid configurations correspond to low global order parameter (vanishing in the thermodynamic limit $N \rightarrow \infty$) with short-range order which is characterised by an exponential decay of correlation functions. On the contrary we showed that, in the solid configuration, systems with pair-wise stochastic forces (here the pABP model) display long-range translational order which is characterised by a non-vanishing translational order correlation function (15a), while systems with particle-wise stochastic forces (here the ABP model) display quasi-long-range translational order which is characterised by an algebraic decay of this same function (15b). In both cases, the global order parameter is high (and finite in the thermodynamic limit $N \rightarrow \infty$).

We observe, consistently with the dynamical approach of Appendix E, for the ABP model that melting occurs between $f = 0.07$ and 0.08 (Fig. H.1(a, c, e)), and for the pABP model between $f = 0.11$ and 0.117 (Fig. H.1(b, d, f)).

We have not provided a theory for the fluctuations of the orientational order $\psi_{6,i}$. In particular, it is yet unknown if systems with fluctuating active stresses may display orientational (quasi)-long-range order and translational short-range order, in the manner of hexatic systems with fluctuating active forces [8, 74, 75].

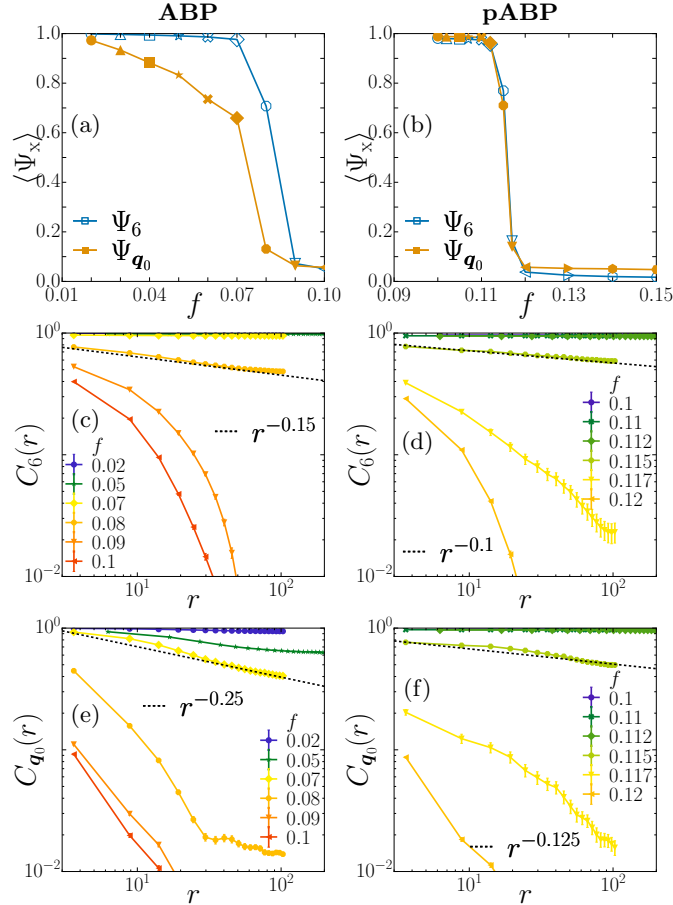


FIG. H.1. (a, b) Global structural order parameters (13) – hexatic order parameter Ψ_6 (blue open symbols) and translational order parameter Ψ_{q_0} (orange full symbols) in steady state as functions of the stochastic force amplitude f . (c, d) Orientational order correlation functions $C_6(r)$, and (e, f) translational order correlations $C_{q_0}(r)$ as functions of space for different stochastic force amplitudes f . We used $N = 16384$ particles for (a, b) and $N = 16384$ or 65536 for (d-g), and persistence time $\tau = 25$. Dashed lines are algebraic functions of distance as guides to the eye. Identical markers between (a), (c), and (e), and between (b), (d), and (f) correspond to identical f , as well as to identical data sets between (c) and (e), and between (d) and (f).